NUMERICAL MODELING OF HYDROTHERMAL CIRCULATION AT OCEAN RIDGES

A THESIS

Presented to

The Faculty of the Division of Graduate

Studies and Research

By

Patricia Lynn Patterson

In Partial Fulfillment

of the Requirements for the Degree

Master of Science in Geophysical Sciences

Georgia Institute of Technology

August, 1976

NUMERICAL MODELING OF HYDROTHERMAL CIRCULATION

AT OCEAN RIDGES

Approved:

Dr. Robert Lowell, Chairman

Dr. Timothy Long

Dr. Kevin Beck

Date approved by Chairman: 8/25/76

ACKNOWLEDGMENTS

I would like to thank Drs. Robert Lowell, Timothy Long, and Kevin Beck, members of my reading committee, for their careful review of the manuscript for this thesis and for their helpful suggestions. I further would like to thank my thesis advisor, Dr. Robert Lowell, for his guidance, availability, patience, and support during the course of my work on this project. Also, I would like to thank Mr. Scott Parks, a fellow student, for his assistance in the computer work.

This project was supported by the National Science Foundation under grant DES 74-00513-A01.

TABLE OF CONTENTS

LIST OF SYMBOLS

A	Non-dimensionalized change in permeability with depth, $\frac{\partial K}{\partial X}$
α	Coefficient of thermal volume expansion of fluid
C	Rate of fluid exchange with ocean
c	Specific heat
D	Non-dimensionalized thickness of porous layer, d/h
DD	Non-dimensionalized width of, and depth to, intrusion, dd/h
d	Thickness of porous layer
dd	Width of, and depth to, intrusion
$\Delta\tau_{\ell}$	Non-dimensionalized increment of time separating τ_{ℓ} and $\tau_{\ell+1}$
ΔX	Non-dimensionalized vertical space increment
ΔY	Non-dimensionalized horizontal space increment
F	Bottom temperature boundary condition, $\frac{\partial T^{o}}{\partial X}$
f	Subscript indicating parameter refers to fluid
h	Linear extent of model
i	Subscript indicating vertical grid point position
j	Subscript indicating horizontal grid point position
K	Non-dimensionalized permeability to vertical fluid flow, k_v/k_r
$\underset{\sim}{k}$	Permeability tensor
k_h	Permeability to horizontal fluid flow
k_r	Reference permeability, 1 Darcy = $0.987 \cdot 10^{-8}$ cm^2
k_v	Permeability to vertical fluid flow
κ	Thermal conductivity of fluid-bearing rock

ℓ	Superscript designating variable at time τ_ℓ
m	Number of horizontal grid points
n	Number of vertical grid points
npp	Number of vertical grid points in porous layer
ν	Kinematic viscosity of fluid
P	Pressure of fluid
p	Ratio of vertical to horizontal permeability, k_v/k_h
'	Superscript designating perturbation component of variable
ψ	Stream function
Q	Heat/distance in z-direction
q	Conductive heat flow through top boundary
R	Non-dimensional quantity, $\frac{k_r(\rho^o c)_f h\alpha g T_o}{\kappa\nu}$
ρ	Density
(s)	Superscript designating value of ψ after s scans by successive overrelation method
s_{max}	Maximum number of scans to be used in determining ψ
T	Temperature
T_r	Temperature below which nonzero permeability exists in porous layer
T_o	Initial temperature of intrusion
t	Time
τ	Non-dimensionalized time, $\frac{\kappa t}{\rho c h^2}$
τ_ℓ	Non-dimensionalized time after ℓ-1th time step $\Delta\tau_{\ell-1}$
θ	Non-dimensionalized perturbation temperature, T'/T_o
θ^o	Non-dimensionalized non-perturbation temperature, T^o/T_o
$\bar{u}_m$	Actual velocity of fluid
$\bar{u}$	Darcy velocity of fluid

V	Volume of fluid exchange with ocean
$\bar{v}$	Non-dimensionalized Darcy velocity of fluid, $\frac{(\rho^o c)_f h\bar{u}}{\kappa}$
w	Relaxation coefficient
X	Non-dimensionalized vertical scale, x/h
x	Vertical reference axis and scale
Y	Non-dimensionalized horizontal scale, y/h
y	Horizontal reference axis and scale
o	Superscript designating non-perturbation component of variable

LIST OF ILLUSTRATIONS

LIST OF ILLUSTRATIONS (cont.)

LIST OF TABLES

SUMMARY

Mean values of ocean-floor heat conduction measured near ridge axes are lower than those predicted by models of a conductively cooling crust. It has been suggested, therefore, that hydrothermal circulation occurs in the oceanic crust and that convective heat transfer from the crust to the ocean accounts for the discrepancy.

In this study two-dimensional, time-dependent, numerical models of a hydrothermal system at an ocean ridge axis were developed. The oceanic crust was modeled as a porous medium for various cases of permeability conditions. The ocean bottom was assumed to be a permeable boundary, but the possibility of convective heat transfer occurring across this boundary was precluded by other assumptions. Initially, a vertical intrusion was assumed to have been emplaced instantaneously at the axis. The hydrothermal history of the system then was examined.

Changes in permeability conditions from homogeneous, isotropic distributions did not alter flow patterns or cooling effects significantly. Conductive heat transfer through the ocean bottom resulting from fluid circulation within the crust was directly proportional to crustal permeability for cases of homogeneous, isotropic permeability, and conductive heat transfer through the ocean bottom became more concentrated at the ridge axis with increasing crustal permeability. Since ocean-floor heat conduction has not been measured closer than five kilometers to a ridge axis, the absence of measurements at the axis, therefore, could

account for the discrepancy between the mean values of heat fluxes measured and those predicted by conductive models. Convective heat transfer through the ocean floor need not be called upon to account for this discrepancy.

CHAPTER I

INTRODUCTION

The first reliable measurements of conductive heat flow through the ocean floor were made in the early 1950's (Revelle and Maxwell 1952), and by the end of the decade enough such measurements had been made for the existence of high fluxes near ocean ridges to be apparent (Von Herzen, 1959). By the mid 1960's, after more measurements near ridges had been made, wide deviations of individual values from the average high were recognized (Lee and Uyeda, 1965; Von Herzen and Langseth, 1966). Recently, measurements involving a dense distribution of data points were made along a profile normal to, and extending five to thirty-five kilometers from, the Galapagos Spreading Center axis (Williams et al., 1974). Although the values were widely scattered with respect to the average, the scatter was not erratic, but approximately sinusoidal with a wavelength of five to seven kilometers.

Attempts to explain the high fluxes began in 1959 when Von Herzen suggested they might be associated with rising limbs of mantle convection cells. Later, the theory of sea-floor spreading (Deitz 1961; Hess 1962) afforded still another possible explanation -- periodic intrusions at ridge axes. In accord with this theory and the evolving concept of plate tectonics, geophysicists began developing mathematical models of a conductively cooling lithosphere, originating at the ridge axis (Langseth et al., 1966; McKenzie, 1967; Sleep, 1969; Sclater and Francheteau, 1970; Parker and Oldenburg, 1973). McKenzie's model, for

example, involved a cooling lithospheric slab, moving at a constant velocity away from an isothermal ridge axis. Figure 1 compares the ocean-floor heat-flux distribution predicted by his application of this model to the Mid-Atlantic Ridge with that of actual data. On the basis of this comparison and those for other ridges, he concluded that intrusions at ridge axes could account for the high heat fluxes and that the mantle under ridges need not be hotter than elsewhere. McKenzie's model, along with all other conductive models, however, predicted heat-flow values near axes much greater than the average measured values.

To account for this discrepancy and to account for the high scatter of measured flux values, Pálmason (1967) proposed that hydrothermal circulation might occur in the oceanic crust at ridge axes. Heat could be convected through the ocean bottom by sea-water entering and leaving through fractures, and this heat transfer would not be detected by thermal-gradient-measuring instruments. Regions of the oceanic crust where fluid flows up would exhibit high values of surface conduction, and regions where fluid flows down, low values. Thus, convection cells could explain the high scatter of values. Detailed studies of heat-flow data collected near ridge axes have supported Pálmason's hypothesis (Talwani et al., 1971; Lister, 1972; Williams et al., 1974).

Besides the anamolous heat fluxes near ridges, the occurrence of other phenomena has been interpreted as evidence for hydrothermal circulation. Pálmason, in fact, was led to the original suggestion after having observed that heat-flow values in the Neovolcanic Zone of Iceland (a surface expression of the Mid-Atlantic Ridge) were controlled by water circulation. He speculated that the situation at submerged ridges might

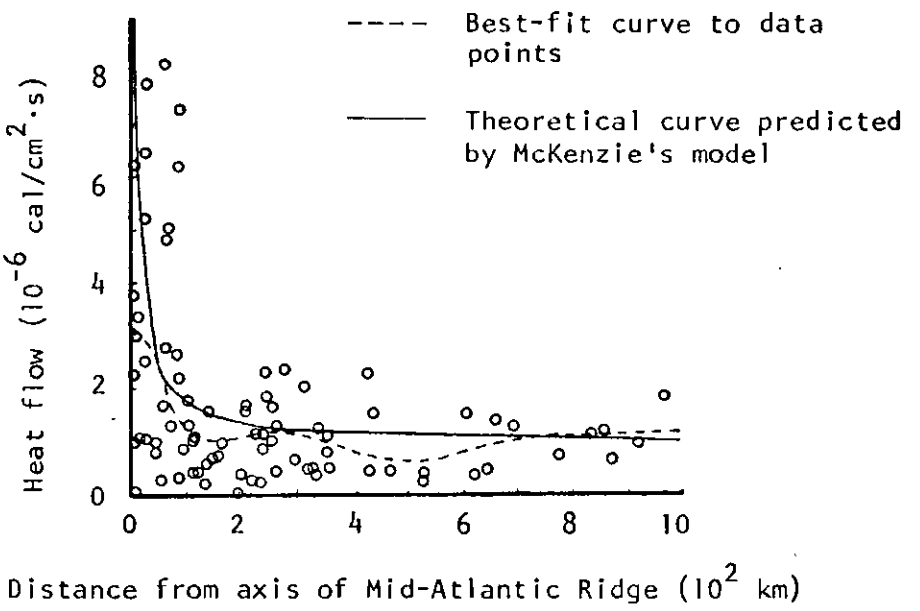

Figure 1. Heat Flow in the Atlantic Ocean [from McKenzie (1967)].

be similar. Others have proposed as evidence phenomena occurring at the submerged ridges themselves: the decay in intensity of magnetic remnance with distance from ridge axes (Irving et al., 1970; Irving, 1970); microearthquake swarms (Sykes, 1971); bottom water temperature anomalies (Williams et al., 1974; Rona et al., 1975); cracks (Ballard, 1975); and several geological and geochemical phenomena [see Wolery and Sleep (1975)]. Wolery and Sleep (1975), however, believe the most conclusive evidence to be the discrepancy between the predicted and observed average heat fluxes.

Modeling of hydrothermal systems at ocean ridges has led to somewhat contradictory conclusions regarding convective heat transfer. Models developed by Bodvarsson and Lowell (1972) have shown that substantial amounts of convective heat loss from the oceanic lithosphere may occur, but recent models developed by Ribando et al. (1976) have shown that no net convective heat loss occurs. The conflicting conclusions may be related to the failure of these models to simulate conditions at the spreading-center axis itself. At the axis horizontal temperature gradients, introduced by near-surface intrusions, and transient effects, resulting from intermittence in the emplacement of these intrusions, could be very important. If Ribando et al.'s conclusion is valid for regions away from the axis, conditions at the axis itself become very important in attempting to explain the discrepancy between the heat fluxes observed and those predicted by conductive models.

The conflicting conclusions regarding convective heat transfer may be related also to the assumed nature of permeability conditions in the oceanic crust. In their models Ribando et al. (1976) assumed that

the oceanic crust acts as a porous medium. If fractures are numerous and interconnecting on a scale sufficiently small compared to that of the model, this is a valid assumption (Muskat, 1937, pp. 7-8). Lister (1974) developed a model for crack propagation, which predicted that interconnected networks of cracks with intercrack spacings of just a few meters may exist at ridge axes; if such networks exist, modeling the crust as a porous medium on the scale of kilometers (as Ribando et al. have done) would be valid. Bodvarsson and Lowell in their models (Bodvarsson and Lowell, 1972; Lowell, 1975), however, assumed that intercrack spacings are on the scale of kilometers. They considered the thermal effects of fluid flow in discrete fracture channels and predicted surface heat fluxes in agreement with actual data. But Ribando et al. with their porous-media models predicted fluxes in agreement with the same data. Closely related to the question of intercrack spacing is that of magnitude of permeability. Lister's model predicted permeabilities to be on the order of $10^{-7}cm^2$, but Ribando et al.'s models predicted values as low as $4.5 \cdot 10^{-12}cm^2$. Inhomogeneities and anisotropies in permeability may be important also. Ribando et al. considered the effects of permeability decreasing with depth but concluded that the existence of such a permeability distribution could not be detected from surface heat-flux measurements. They did not, however, consider the effects of anisotropic permeability.

The purpose of this study will be to examine the effects of some of the conditions not included in the earlier work of others. Modeling will begin with the emplacement of a high-temperature intrusion into a porous layer of oceanic crust at a ridge axis. The time-dependent effects of the resulting horizontal temperature gradients on the development of

the hydrothermal system will be investigated. Different cases of crustal permeability conditions will be considered, including: homogeneous, isotropic permeabilities; non-homogeneous, isotropic permeabilities; and homogeneous, anisotropic permeabilities.

The region modeled will involve only the immediate vicinity of the ridge axis. The surface heat fluxes obtained will not be compared with actual data since none exists for regions closer than five kilometers to an axis (Williams et al., 1974). (Measuring instruments must be embedded in sediments, and sediments are absent at axes.) It is hoped, nevertheless, that the results will provide some insight into the nature of actual hydrothermal conditions at ridge axes.

CHAPTER II

DESCRIPTION OF MODEL

Figure 2 shows the basic model with initial and boundary conditions. The model is two-dimensional, extending indefinitely in the positive and negative z-directions. The xy plane cuts a cross-section of the oceanic crust perpendicular to the ridge axis. The xz plane corresponds to the ridge axis, and symmetry with respect to this plane simplifies modeling. The yz plane corresponds to the ocean bottom. The cross-hatched region represents a rectangular intrusion, having been emplaced instantaneously at time $t = 0$, with initial temperature T_o. The region $0 \leq x < d$ is porous and water saturated, and the region $d \leq x \leq h$ is non-porous. The permeability, $\underset{\sim}{k}$, in the region $0 \leq x < d$ is a function of temperature, T, as follows:

$$\underset{\sim}{k}(x,y) = \begin{cases} 0 & \text{if } T(x,y) \geq T_r \\ \underset{\sim}{k}(x) & \text{if } T(x,y) < T_r \end{cases}.$$

T_r is the temperature below which a permeable network of cracks forms. (A detailed treatment of permeability variations due to thermo-elastic and chemical processes is beyond the scope of this study.) Permeability will not vary horizontally within regions where $T(x,y) < T_r$, but in some cases will be anisotropic, so is designated as a tensor, $\underset{\sim}{k}$. When permeability varies vertically, the rate of variation will be assumed to be constant.

Fluid-flow boundary conditions, where $\bar{u}$ is the Darcy velocity of

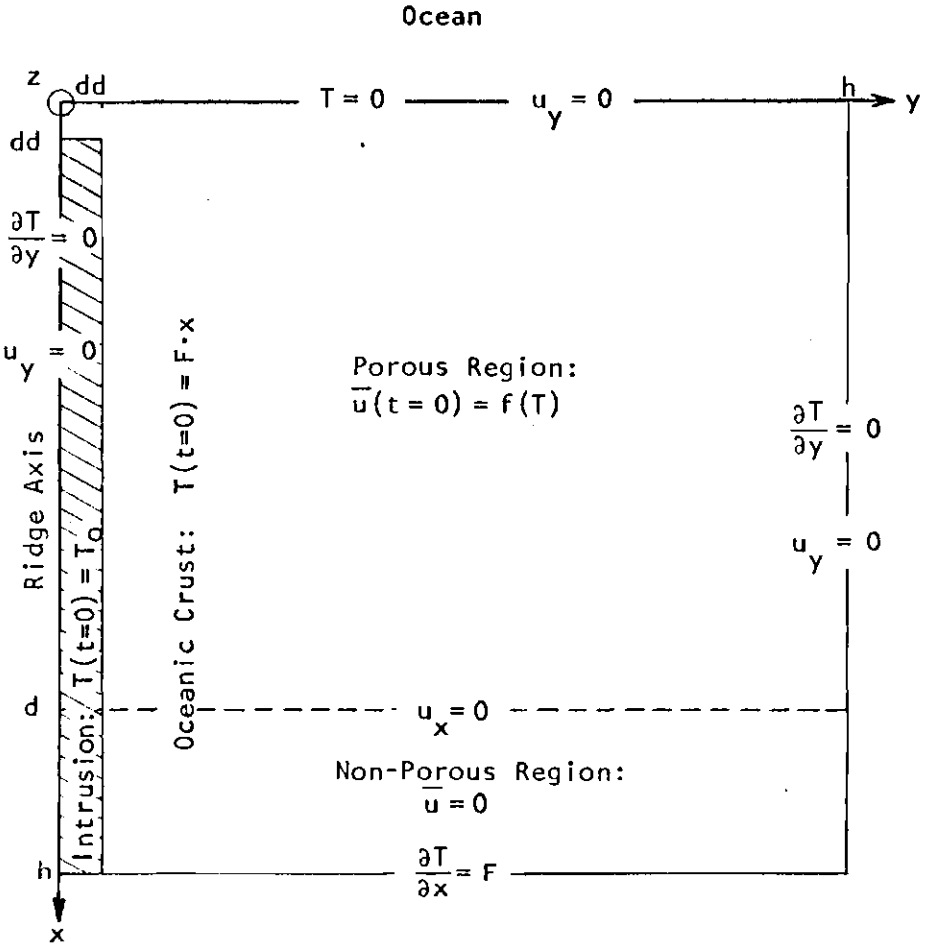

Figure 2. Basic Model with Initial and Boundary Conditions.

the fluid,[1] simulate convection cell boundaries. These cell boundaries will be displaced inward, out of impermeable regions where $T \geq T_r$. Velocity components perpendicular to these impermeable regions will be set equal to zero. At the top boundary, fluid exchange with an assumedly free-standing fluid occurs, so there is no horizontal flow (Lapwood, 1948). The top boundary temperature condition assumes the ocean is a perfect heat sink. The left and right boundary temperature conditions assume perfect insulation, the left by reason of symmetry. The bottom boundary condition assumes a constant heat flux so that the temperature field at $t < 0$ remains constant at $F \cdot x$. The initial velocity field will derive from the initial temperature distribution.

The fundamental equations for the model require the conservation of fluid mass, heat energy, and fluid momentum and relate fluid density to temperature.

The equation for conservation of fluid mass is:

$$\bar{\nabla} \cdot \bar{u} = 0, \tag{1}$$

where the fluid is assumed to be homogeneous and incompressible. This equation requires that the net amount of fluid flowing through a closed volume equals zero.

---

[1]The Darcy velocity at a point is the average velocity over a macroscopic area, $\Delta x \Delta y$, surrounding the point:

$$\bar{u}(x,y) = \frac{\int_{x-\Delta x/2}^{x+\Delta x/2} \int_{y-\Delta y/2}^{y+\Delta y/2} \bar{u}_m(x,y)\,dx\,dy}{\Delta x \Delta y},$$

where u_m is actual velocity. Description by means of Darcy velocity is necessary when considering a porous medium, where flow is such that actual fluid velocity at a point is not easily related to physical forces.

The equation for conservation of heat energy is:

$$\rho c \frac{\partial T}{\partial t} = \kappa \nabla^2 T - (\rho c)_f \bar{u} \cdot \bar{\nabla} T, \tag{2}$$

where specific heat, c, and thermal conductivity, κ, are assumed to be constant and the fluid and porous rock are assumed to be in thermodynamic equilibrium, i.e., at an interface between the two, both are assumed to be at the same temperature. This equation requires that the increase in heat per time per unit volume ($\rho c \, \partial T/\partial t$) equals the heat conducted per time into the unit volume ($\kappa \nabla^2 T$) plus the heat convected per time into the unit volume [$-(\rho c)_f \, \bar{u} \cdot \bar{\nabla} T$]. Heat generated within the model through friction, etc., is assumed to be negligible.

The equation for conservation of fluid momentum is:

$$-\bar{\nabla} P + \rho_f \bar{g} - \rho_f \nu \underset{\sim}{k}^{-1} \cdot \bar{u} = 0, \tag{3}$$

where P is pressure, $\bar{g}$ is the acceleration of gravity, ν is kinematic viscosity, and $\underset{\sim}{k}^{-1}$ is the inverse of the permeability tensor. Kinematic viscosity will be assumed to remain constant. This equation is valid only if fluid flow is laminar and if the effective grain size of the porous rock is much smaller than the scale at which fluid flow will be considered. This equation requires that the pressure-gradient force per unit volume of fluid ($-\bar{\nabla} P$), the gravitational force per unit volume ($\rho_f \bar{g}$), and the viscous force per unit volume ($-\rho_f \nu \underset{\sim}{k}^{-1} \cdot \bar{u}$) cancel. No inertial force term ($\rho_f \frac{d\bar{u}}{dt}$) is involved since inertial forces are negligible compared to internal friction resistances (viscous forces) in a porous medium (Straus, 1974).

The equation of state for the fluid is:

$$\rho_f = \rho_f^o \ [1 - \alpha(T - T^o)], \tag{4}$$

where density ρ_f exists at temperature T when ρ_f^o exists at T^o. This equation assumes fluid density and temperature to be linearly related through the constant α, the coefficient of thermal volume expansion of the fluid.

The solutions to these fundamental equations in terms of temperature, T, and velocity, $\bar{u}$, will be used in determining other physical quantities of interest. These quantities and their equations are: heat conduction through the top boundary:

$$q(y,t) = \kappa[\frac{\partial T(y,t)}{\partial x}]_{x=o}; \tag{5}$$

total heat conducted through the top boundary by time t:

$$Q(t) = \int_o^h \int_o^t q(y,t)dydt; \tag{6}$$

total heat in the model:

$$Q(t) = c \int_o^h \int_o^h T(x,y,t)dxdy; \tag{7}$$

rate of fluid exchange through the top boundary:

$$C(t) = \frac{1}{2} \int_o^h |u_x(y,t)|_{x=o} dy; \tag{8}$$

and total volume of fluid exchange by time t:

$$V(t) = \int_{o}^{t} C(t)dt. \qquad (9)$$

CHAPTER III

SOLUTION OF EQUATIONS

Solutions to all equations will be obtained in terms of perturbations from the conditions existing at $t < 0$. These conditions are depicted in Figure 2 if the intrusion is omitted. All velocities will be assumed to be zero in this state. For times $t \geq 0$ each function will be represented by two components: a pre-intrusion component equivalent to the value of the function at $t < 0$ and a perturbation component equivalent to the difference between the function value at time t and its value at $t < 0$. The functions are thusly represented:

$$\bar{u} = \bar{u}^{o} + \bar{u}' \approx \bar{u}'$$

$$\rho_f = \rho_f^{o} + \rho_f'$$

$$T = T^{o} + T'$$

$$P = P^{o} + P',$$

where the pre-intrusion components are designated with zero superscripts and the perturbation components with primes.

Substituting this representation into equations (1) through (4) gives:

$$\bar{\nabla} \cdot \bar{u}' = 0 \tag{10}$$

$$\rho c \frac{\partial T'}{\partial t} = \kappa \nabla^2 T' - (\rho^{o} c)_f \, \bar{u}' \cdot \bar{\nabla}(T^{o} + T') \tag{11}$$

$$-\bar{\nabla}(P^{o} + P') + (\rho^{o} + \rho')_{f}\,\bar{g} - \rho_{f}\,\nu\,\underset{\sim}{k}^{-1}\cdot\bar{u}' = 0 \qquad (12)$$

$$\rho_{f}' = -\,\rho_{f}^{o}\,\alpha T'. \qquad (13)$$

Here the Boussinesq approximation was employed according to which density variations are considered significant only in their generation of buoyancy forces. Thus ρ_f' appears only in the gravity force term and in the equation of state. This approximation will be valid as long as density changes are small compared to ρ_f^o (Richter, 1973, pp. 232-233).

Eliminating the pressure terms by taking the curl of vector equation (12), combining the resulting equation with equation (13), and simplifying gives:

$$\alpha g\,\frac{\partial T'}{\partial y} + \frac{\nu u_y'}{k_h^2}\,\frac{\partial k_h}{\partial x} - \frac{\nu}{k_h}\,\frac{\partial u_y'}{\partial x} + \frac{\nu}{k_v}\,\frac{\partial u_x'}{\partial y} = 0, \qquad (14)$$

where k_h and k_v are tensor components, permeability to horizontal flow and permeability to vertical flow, respectively. No term involving $\partial k_v/\partial y$ appears since $\underset{\sim}{k}$ will not vary horizontally within permeable regions.

Boundary and initial conditions for these perturbation equations are:

$$T'(0,y) = \frac{\partial T'(x,0)}{\partial y} = \frac{\partial T'(x,h)}{\partial y} = \frac{\partial T'(h,y)}{\partial x} = 0; \qquad (15)$$

$$u_y'(0,y) = u_y'(x,0) = u_y'(x,h) = u_x'(d,y) = 0, \qquad (16)$$

when $T < T_r$ everywhere in the region $0 \leq x < d$; and

$$T'(t=0) = \begin{cases} T_o - F \cdot x & \text{at and inside the intrusion} \\ 0 & \text{outside the intrusion} \end{cases} . \qquad (17)$$

The equations and boundary and initial conditions will be further modified by introducing the non-dimensional parameters:

$$\begin{aligned} X &= x/h \\ Y &= y/h \\ D &= d/h \\ DD &= dd/h \\ \tau &= \frac{\kappa t}{\rho c h^2} \\ \bar{v} &= \frac{(\rho^o c)_f h \bar{u}'}{\kappa} \\ \theta^o &= T^o/T_o \\ \theta &= T'/T_o \\ \theta_r &= T_r/T_o \\ p &= k_v/k_h \\ K &= k_v/k_r \\ R &= \frac{k_r (\rho^o c)_f \, h \alpha g \, T_o}{\kappa \nu} , \end{aligned} \qquad (18)$$

where k_r is a reference permeability value. Substituting these parameters into equations (10), (11), and (14) gives the dimensionless equations:

$$\bar{\nabla} \cdot \bar{v} = 0 \qquad (19)$$

$$\frac{\partial \theta}{\partial \tau} = \nabla^2 \theta - \bar{v} \cdot \bar{\nabla} (\theta^o + \theta) \qquad (20)$$

$$KR\frac{\partial\theta}{\partial Y} + \frac{\partial v_x}{\partial Y} - p\frac{\partial v_x}{\partial X} + \frac{pv_yA}{K} = 0, \tag{21}$$

where $A = \partial K/\partial X$. Boundary and initial conditions become:

$$\theta(0,Y) = \frac{\partial\theta(X,0)}{\partial Y} = \frac{\partial\theta(X,1)}{\partial Y} = \frac{\partial\theta(1,Y)}{\partial X} = 0; \tag{22}$$

$$v_y(0,Y) = v_y(X,0) = v_y(X,1) = v_x(D,Y) = 0, \tag{23}$$

when $\theta < \theta_r$ everywhere in the region $0 \leq X < D$; and

$$\theta(\tau=0) = \begin{cases} 1 - \theta^o & \text{at and inside the intrusion} \\ 0 & \text{outside the intrusion} \end{cases}. \tag{24}$$

The fundamental equations will be modified still further by introducing a stream function, ψ, such that:

$$v_x = -\partial\psi/\partial Y \qquad \text{(a)}$$

$$v_y = \partial\psi/\partial X. \qquad \text{(b)} \tag{25}$$

This function automatically satisfies equation (19) and provides a simple means of depicting fluid flow, since fluid flow is parallel to streamlines.[2] Substituting equations (25) into equation (21)

---

[2]Streamlines are lines of constant ψ and are thus derived from the equation:

$$d\psi = \frac{\partial\psi}{\partial X}dX + \frac{\partial\psi}{\partial Y}dY = 0.$$

which reduces to:

$$\frac{v_Y}{v_X} = \left(\frac{\partial Y}{\partial X}\right)_{\psi=\text{constant}}.$$

Thus streamlines are inclined in the direction of fluid velocity (Neumann and Pierson, 1966, p. 151).

gives:

$$KR \frac{\partial \theta}{\partial Y} - \frac{\partial^2 \psi}{\partial Y^2} - p \frac{\partial^2 \psi}{\partial X^2} + \frac{pA}{K} \frac{\partial \psi}{\partial X} = 0 \tag{26}$$

for the fluid flow equation. Boundary conditions from equation (23) become:

$$\frac{\partial \psi(0,Y)}{\partial X} = 0 \tag{27}$$

for the top boundary, and

$$\psi(X,0) = \psi(X,1) = (0,Y) = 0 \tag{28}$$

for the other boundaries which lie along the outermost streamline of the convection cell. When the cell boundary must be displaced inward out of impermeable regions where $\theta \geq \theta_r$, the condition $\psi = 0$ will be applied along the boundary between the permeable and impermeable regions.

Solutions will be obtained to equations (20), (25), and (26) by finite difference methods. Such methods have been commonly employed in solving related problems of heat transport in porous media (Donaldson, 1962; Elder, 1967; Torrance, 1968; Holst and Aziz, 1972a, 1972b; Horne and O'Sullivan, 1974).

A network of n x m grid points is superimposed on the XY coordinate axes, as shown in Figure 3, where $n = m = 20$ and $\Delta X = \Delta Y = 1/20$. The time dimension has been represented here as a third spatial dimension. The differential equations will be approximated by algebraic equations

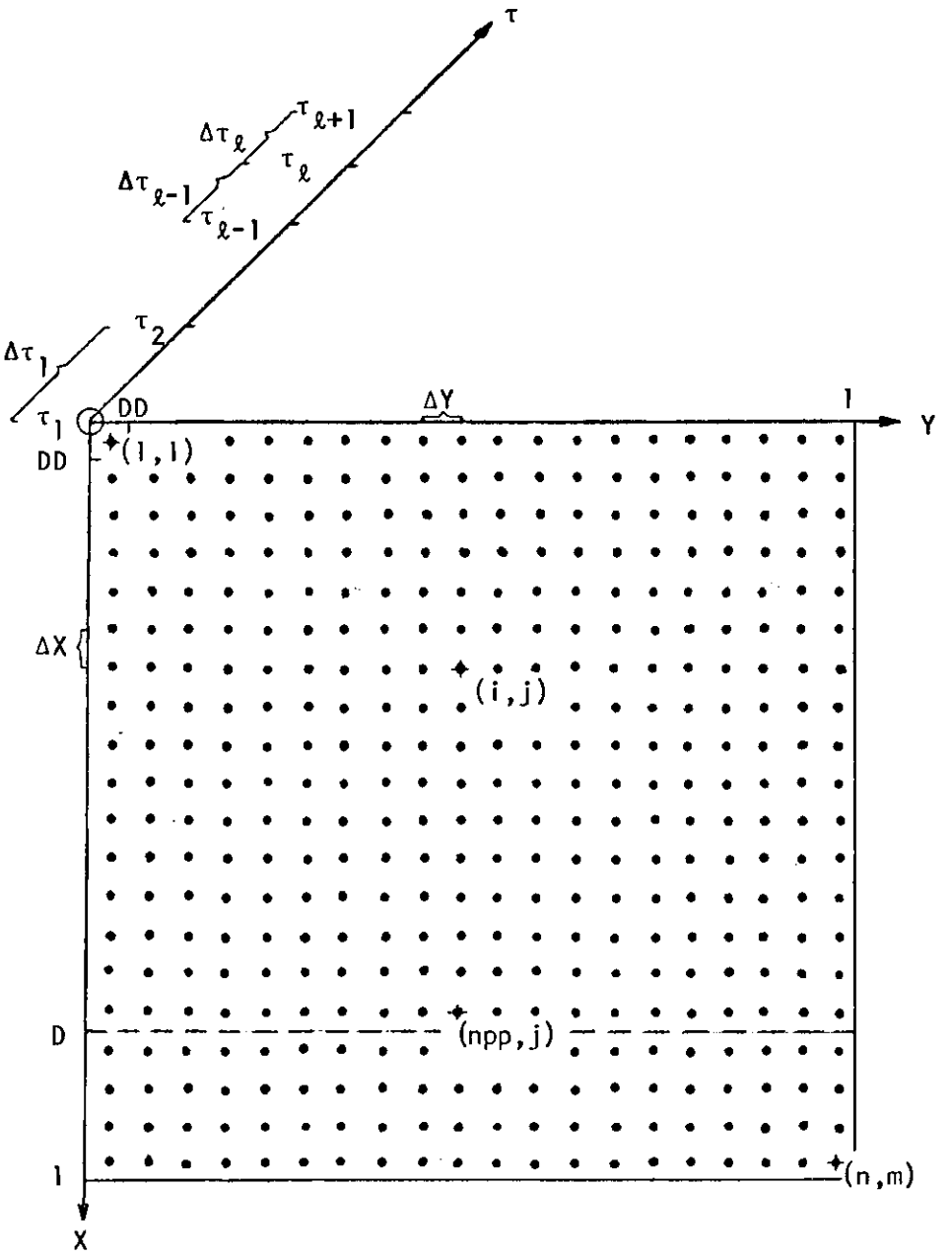

Figure 3. Two-Dimensional Network of Grid Points with Time Axis.

derived from truncated Taylor's expansions about individual grid points.[3]

---

[3]Let f be a function analytic over the grid space. The values of f at points (i-1,j) and (i+1,j) are related to the value of f at the adjacent point (i,j) by the Taylor's expansions:

$$f_{i-1,j} = f_{i,j} - \Delta X \frac{\partial f_{i,j}}{\partial X} + \frac{(\Delta X)^2}{2!} \frac{\partial^2 f_{i,j}}{\partial X^2} - \frac{(\Delta X)^3}{3!} \frac{\partial^3 f_{i,j}}{\partial X^3} + \frac{(\Delta X)^4}{4!} \frac{\partial^4 f_{i,j}}{\partial X^4} + \ldots,$$

and

$$f_{i+1,j} = f_{i,j} + \Delta X \frac{\partial f_{i,j}}{\partial X} + \frac{(\Delta X)^2}{2!} \frac{\partial^2 f_{i,j}}{\partial X^2} + \frac{(\Delta X)^3}{3!} \frac{\partial^3 f_{i,j}}{\partial X^3} + \frac{(\Delta X)^4}{4!} \frac{\partial^4 f_{i,j}}{\partial X^4} + \ldots.$$

From these equations finite difference approximations for first- and second-order derivatives will be obtained. Rearranging the first equation,

$$\frac{\partial f_{i,j}}{\partial X} = \frac{f_{i,j} - f_{i-1,j}}{\Delta X} + \left(\frac{\Delta X}{2!} \frac{\partial^2 f_{i,j}}{\partial X^2} - \frac{(\Delta X)^2}{3!} \frac{\partial^3 f_{i,j}}{\partial X^3} + \frac{(\Delta X)^3}{4!} \frac{\partial^4 f_{i,j}}{\partial X^4} + \ldots \right);$$

rearranging the second equation,

$$\frac{\partial f_{i,j}}{\partial X} = \frac{f_{i+1} - f_{i,j}}{\Delta X} - \left(\frac{\Delta X}{2!} \frac{\partial^2 f_{i,j}}{\partial X^2} + \frac{(\Delta X)^2}{3!} \frac{\partial^3 f_{i,j}}{\Delta X^3} + \frac{(\Delta X)^3}{4!} \frac{\partial^4 f_{i,j}}{\partial X^4} + \ldots \right);$$

rearranging the difference between the first and second equations,

$$\frac{\partial f_{i,j}}{\partial X} = \frac{f_{i+1,j} - f_{i-1,j}}{2\Delta X} + 2 \left(\frac{(\Delta X)^2}{3!} \frac{\partial^3 f_{i,j}}{\partial X^3} + \ldots \right); \text{ and}$$

rearranging the sum of the two equations,

$$\frac{\partial^2 f_{i,j}}{\partial X^2} = \frac{f_{i-1,j} - 2f_{i,j} + f_{i+1,j}}{(\Delta X)^2} + 2 \left(\frac{(\Delta X)^2}{4!} \frac{\partial^4 f_{i,j}}{\partial X^4} + \ldots \right).$$

To obtain the finite difference approximations for the derivatives, the terms in parenthesis are dropped (Carnahan et al., 1969, pp. 430-431).

Solutions will be obtained at each grid point at discrete times τ_ℓ, where τ_ℓ is the time after the ℓ-1th time step $\Delta\tau_{\ell-1}$. Solutions should be thought of as averages over increments of area surrounding grid points. The one-dimensional boundary conditions, however, will be assumed to hold along two-dimensional strips of width ΔX or ΔY. (Boundary conditions in finite difference form are discussed in Appendix A.)

Based upon the approximations derived in footnote 3, equations (26), (25) and (20) in finite difference form are:

$$K_i^\ell R \frac{(\theta_{i,j+1}^\ell - \theta_{i,j-1}^\ell)}{2\Delta Y} - \frac{(\psi_{i,j-1}^\ell - 2\psi_{i,j}^\ell + \psi_{i,j+1}^\ell)}{(\Delta Y)^2} - p \frac{(\psi_{i-1,j}^\ell - 2\psi_{i,j}^\ell + \psi_{i+1,j}^\ell)}{(\Delta X)^2} + \frac{pA}{K_i} \frac{(\psi_{i+1,j}^\ell - \psi_{i-1,j}^\ell)}{2\Delta X} = 0 \quad (29)$$

$$v_{x_{i,j}}^\ell = - \frac{\psi_{i,j+1}^\ell - \psi_{i,j}^\ell}{\Delta Y} \quad \text{(a)}$$

$$v_{y_{i,j}}^\ell = \frac{\psi_{i,j}^\ell - \psi_{i-1,j}^\ell}{\Delta X} \quad \text{(b)} \quad (30)$$

$$\frac{\theta_{i,j}^{\ell+1} - \theta_{i,j}^\ell}{\Delta\tau_\ell} = \frac{\theta_{i+1,j}^\ell - 2\theta_{i,j}^\ell + \theta_{i-1,j}^\ell}{(\Delta X)^2} + \frac{\theta_{i,j+1}^\ell - 2\theta_{i,j}^\ell + \theta_{i,j-1}^\ell}{(\Delta Y)^2} - \left\{ \begin{array}{ll} v_{x_{i,j}}^\ell \dfrac{(\theta_{i,j}^\ell - \theta_{i-1,j}^\ell)}{\Delta X} & \text{if } v_{x_{i,j}}^\ell > 0 \\ v_{x_{i,j}}^\ell \dfrac{(\theta_{i+1,j}^\ell - \theta_{i,j}^\ell)}{\Delta X} & \text{if } v_{x_{i,j}}^\ell \leq 0 \end{array} \right\} - v_{x_{i,j}}^\ell \frac{\partial\theta^o}{\partial X}$$

$$- \begin{cases} v^{\ell}_{y_{i,j}} \dfrac{(\theta^{\ell}_{i,j} - \theta^{\ell}_{i,j-1})}{\Delta Y} & \text{if } v^{\ell}_{y_{i,j}} > 0 \\ v^{\ell}_{y_{i,j}} \dfrac{(\theta^{\ell}_{i,j+1} - \theta^{\ell}_{i,j})}{\Delta Y} & \text{if } v^{\ell}_{y_{i,j}} \leq 0 \end{cases} , \qquad (31)$$

where the subscripts designate the spatial position of the function on the grid network and the superscripts, ℓ and $\ell+1$, designate the function at times τ_{ℓ} and $\tau_{\ell+1}$, respectively. The form of the velocity terms in equation (31) derives from stability requirements (Torrance, 1968). Also, the magnitude of $\Delta\tau_{\ell}$ is limited by the stability requirement:

$$\Delta\tau_{\ell} \leq \min_{i,j} \left[\frac{|v^{\ell}_{x_{i,j}}| + |v^{\ell}_{y_{i,j}}|}{\Delta X} + \frac{4}{(\Delta X)^2} \right]^{-1} \qquad (32)$$

(Torrance, 1968). The satisfaction of these stability requirements insures that heat flows from higher to lower temperature points (Dusinberre, 1961, pp. 13-16).

Solutions to equations (29) through (31) will be obtained as follows. Beginning at $\tau_1 = 0$, equation (29) will be solved for ψ^1 from the known temperature (initial) conditions:

$$\theta^{1}_{i,j} = \begin{cases} 1 - \dfrac{\partial\theta^{o}}{\partial X}(i-1)\Delta X & \text{for } j=1 \\ 0 & \text{for } j=2,3,\ldots,m \end{cases} \Bigg\} \text{ and for } i=2,3,\ldots,n. \qquad (33)$$

Next, Equations (30) will be solved for v^{1}_{x} and v^{1}_{y}. The magnitude of

$\Delta\tau_1$, then will be defined as nine-tenths (for safety) its maximum allowable value for stability from equation (32). Using this value of $\Delta\tau_1$, equation (31) will be solved for θ^2 from the known temperature and velocity fields, θ^1 and $\bar{v}^1$. By thus advancing in a stepwise manner through time, solutions may be obtained (through suitable choice of $\Delta\tau_{\ell-1}$) at any desired time τ_ℓ.

Solutions to equation (29) for ψ will be obtained by the method of successive overrelaxation (Young, 1954). Details of this method are given in Appendix A.

Solutions to equations (5) through (9) will involve perturbation and finite difference representation also. For the perturbation heat conduction through the top boundary, equation (5) becomes:

$$q'_j(t^{\ell+1}) = \frac{T_o \kappa \theta^{\ell+1}_{2,j}}{h\Delta X}, \tag{34}$$

where $t^{\ell+1}$ is the dimensionalized representation of $\tau_{\ell+1}$. For the total perturbation heat conducted through the top boundary by time $t^{\ell+1}$, equation (6) becomes:

$$Q'(t^{\ell+1}) = T_o \rho c h^2 \sum_{r=1}^{\ell+1} \sum_{j=1}^{m} \theta^r_{2,j} \Delta\tau_r. \tag{35}$$

For the total perturbation heat in the model, equation (7) becomes:

$$Q'(t^{\ell+1}) = T_o \rho c h^2 \Delta X \Delta Y \sum_{j=1}^{m} \sum_{i=1}^{n} \theta^{\ell+1}_{i,j}. \tag{36}$$

For the rate of fluid exchange through the top boundary, equation (8) becomes:

$$C(t^{\ell}) = \frac{\kappa \Delta X}{2(\rho^{o}c)_{f}} \sum_{j=1}^{m} v_{1,j}^{\ell}. \tag{37}$$

For the total volume of fluid exchange by time t^{ℓ}, equation (9) becomes:

$$V(t^{\ell}) = \frac{h^{2}\rho c}{\kappa} \sum_{r=1}^{\ell} C(t^{r})\Delta\tau_{r}. \tag{38}$$

Numerical solutions to all finite difference equations were obtained using a Control Data Corporation CYBER 74 computer. Programming uses the FORTRAN Extended language and is explained in Appendix C.

CHAPTER IV

APPLICATION OF MODEL

The duration of modeling was from t = 0 to t = 15000 years. Parameters held constant throughout all modeling were:

the fluid-bearing rock properties:

density, $\rho = 3$ gr/cm^3

specific heat, $c = 0.25$ cal/°C·gr

thermal conductivity, $\kappa = 0.01$ cal/°C·cm·s

the fluid properties:

density, $\rho_f^o = 1$ gr/cm^3

specific heat, $c_f = 1$ cal/°C·gr

kinematic viscosity, $\nu = 0.01$ cm^2/s

coefficient of thermal volume expansion, $\alpha = 1.6 \cdot 10^{-4}$/°C

the linear extent of the model, h = 4 km

the width of, and depth to, the intrusion, dd = 0.2 km

the initial temperature of the intrusion, $T_o = 1200$°C

the temperature below which non-zero permeability exists in the porous layer, $T_r = 690$°C. (Lister, 1974), and

the bottom temperature boundary condition, $F = \frac{\partial T^o}{\partial X} = 100$°C/km.

Parameters varied for different cases of modeling were the depth of the porous layer, d, and its permeability, $\underset{\sim}{k}$. By this variation, results were obtained for five general cases of crustal permeability conditions:

(1) zero permeability everywhere; (2) homogeneous, isotropic permeability everywhere; (3) isotropic permeability linearly decreasing from a maximum value at the top boundary to zero at the bottom boundary; (4) homogeneous, isotropic permeability to a depth less than h; and (5) homogeneous, anisotropic permeability everywhere. Specific cases are identified in Table 1.

Spooner and Fyfe (1973) have predicted that fluid circulation near ocean ridges extends to a depth of 5 km, i.e., that convection cells extend 5 km vertically. Williams et al. (1974), on the other hand, have evidence that convection cells extend approximately 3 km horizontally. The value of h for this study was chosen to be an average of these two estimates.

Based on geologic data recently collected at the axis of the Mid-Atlantic Ridge (Bellaiche et al., 1974), Moore et al. (1974) have developed a model for extrusion and rifting at this axis. Their model estimates an intrusion periodicity of 14000 years and an associated average yearly spreading rate of 2.2 cm. These conditions, along with their estimated intrusion geometry, are in line with the basic model of this study when dd is chosen to be 0.2 km. The emplacement of an intrusion of this width every 15000 years corresponds to an average yearly spreading rate of 2.7 cm. dd was chosen to be 0.2 km so as to correspond to the non-dimensionalized distance ΔX. This correspondence facilitated its finite difference representation.

The regional geothermal gradient in Iceland is approximately 100°C/km (Pálmason, 1967). Since Iceland is part of an ocean ridge, this gradient

Table 1. Cases Modeled

Case	d	$k_{v_{max}}$	$\frac{\partial k_v}{\partial x}$	p
1	0			
2	4		0	1
a		0.1		
b		0.0275		
c		0.01		
d		0.0075		
e		0.005		
f		0.001		
3	4	0.01	$-\frac{0.01}{4}$	1
4		0.01	0	1
a	2			
b	3			
5	4	0.01	0	
a				2
b				3
c				10

Explanation:

d is depth of porous layer in km.

$k_{v_{max}}$ is permeability to vertical flow at top boundary in Darcies (1 Darcy = $0.987 \cdot 10^{-8}$ cm^2).

$\frac{\partial k_v}{\partial x}$ is change in permeability with depth in Darcies/km.

p is ratio of permeability to vertical flow to permeability to horizontal flow.

was chosen to be the value of F, the bottom temperature boundary condition and the pre-intrusion temperature gradient for the model. This gradient corresponds to a non-perturbation heat flux $q^o = 10 \cdot 10^{-6} cal/s \cdot cm^2$. All heat-flow results will be given in terms of perturbation values [q' from equation (34)] and must be added to q^o to obtain actual measurable quantities. (Isotherms for the initial temperature field for this value of F are shown in Figure 4.)

The range of permeability conditions modeled centers around K = 0.01. This value was chosen so as to lie roughly between the two extreme orders of magnitude predicted by Lister (1974) and Ribando et al. (1976).

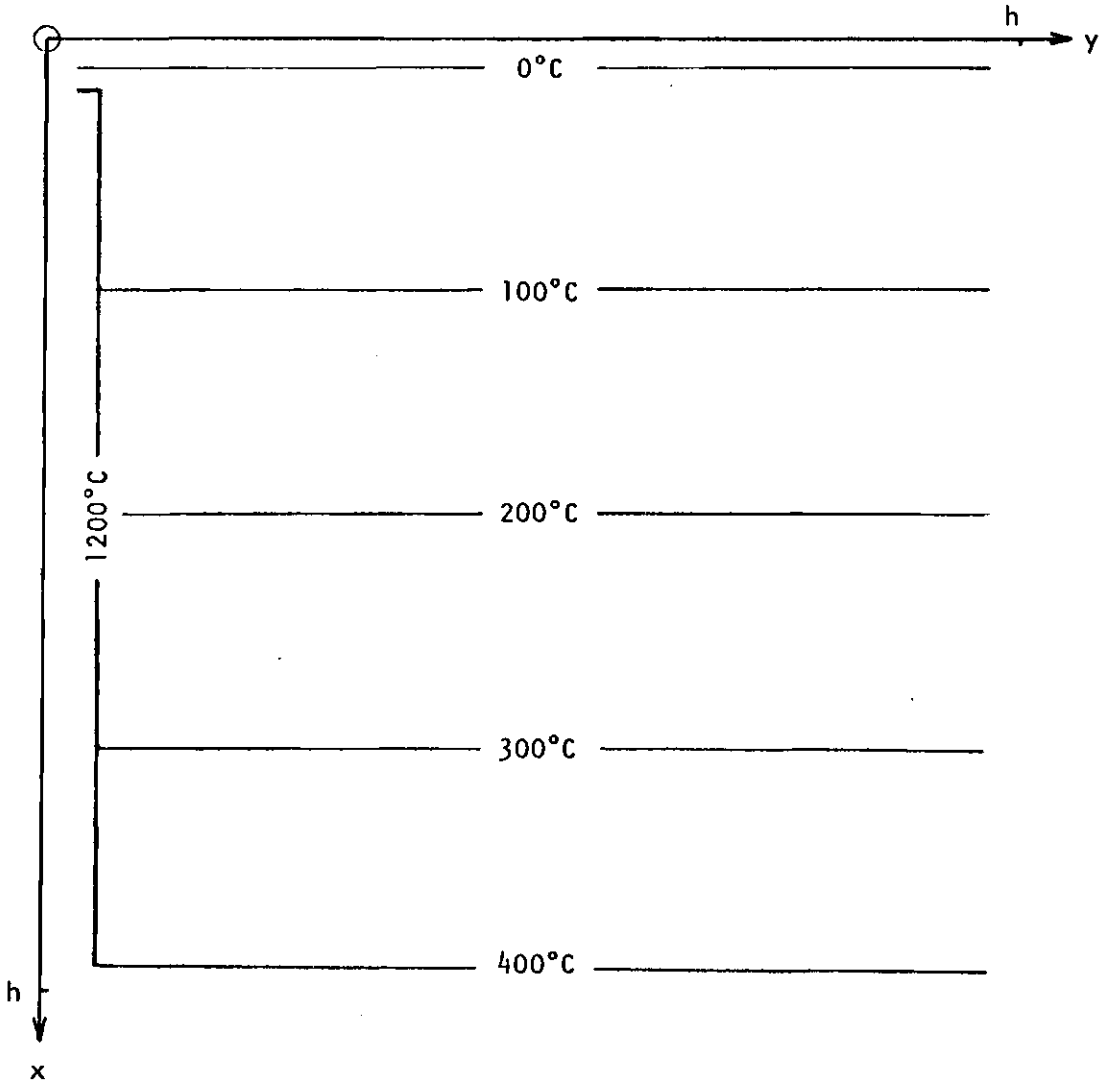

Figure 4. Initial Temperature Field.

CHAPTER V

PRESENTATION OF RESULTS

Principal results are given in Figures 5 through 16 and in Table 2. Figure 5 shows the time development of the temperature field, T, for the conductive case. Part (a) shows isotherms at t = 6000 years, along with isotherms at t = 0 for comparison. Steep temperature gradients initially at the intrusion boundary have decreased, while gradients outside and near the intrusion have increased. Part (b) shows isotherms at t = 15000 years, along with those at t = 6000 years. Near the axis isotherms have moved closer to their pre-intrusion positions, and gradients have decreased. Further from the axis isotherms have moved upward from their pre-intrusion positions, and gradients have increased.

The temporal changes in vertical gradients near the surface are reflected in the perturbation surface heat flux, q'. The solid lines of Figure 6 show q' as a function of distance from the ridge axis at t = 1-,3-,6-, and 15000 years for this non-convective case. At the axis q' decreases with time, but at points away from the axis q' increases to a maximum and then decreases with time. The closer a point to the axis, the sooner it reaches its maximum. Spatially, q' always decreases with distance from the axis.

Figure 7 (for case 2c) shows features typical of the time development of a hydrothermal system. The dashed lines represent streamlines, parallel to which fluid flows. The direction of flow is up near

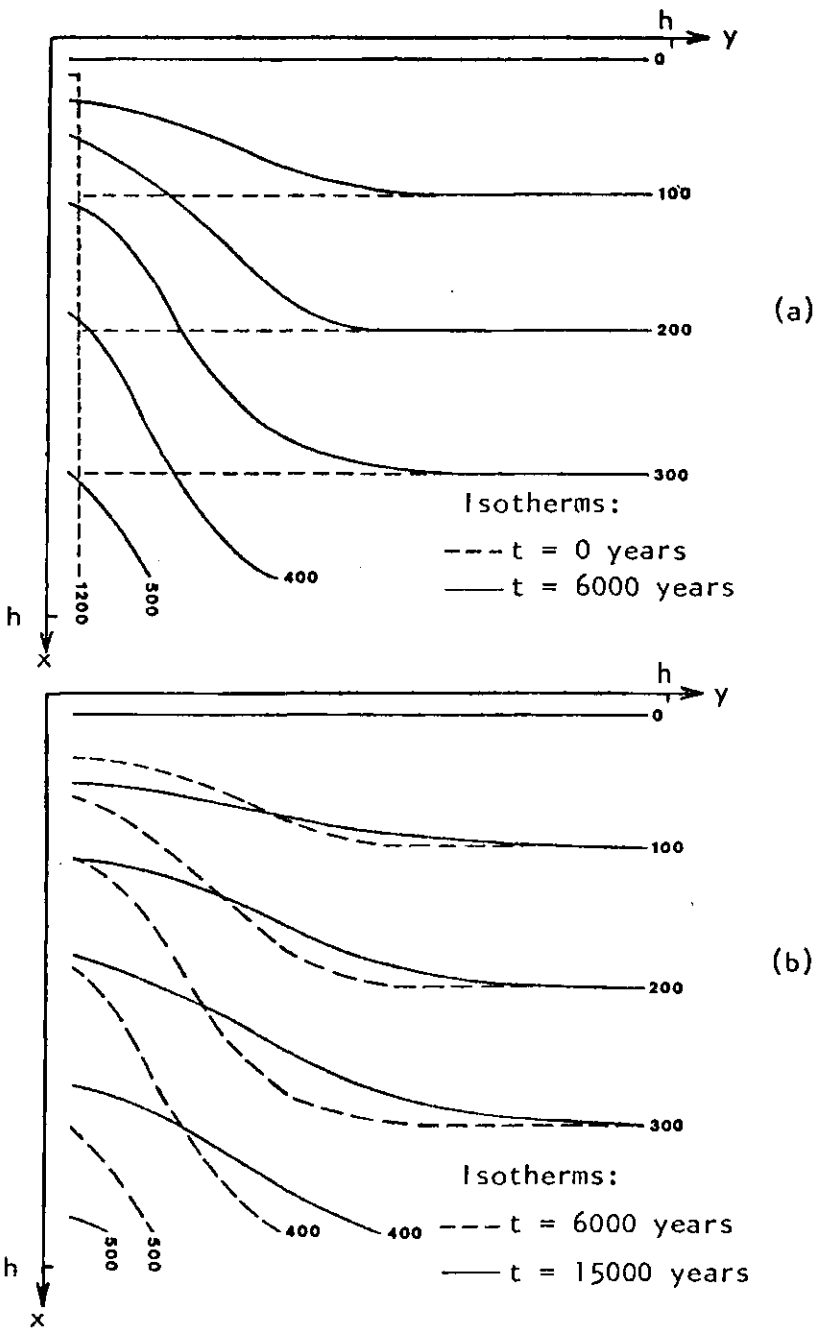

Note: Isotherms are designated in °C.

Figure 5. Time Development of Temperature Field for Conductive Case (Case 1).

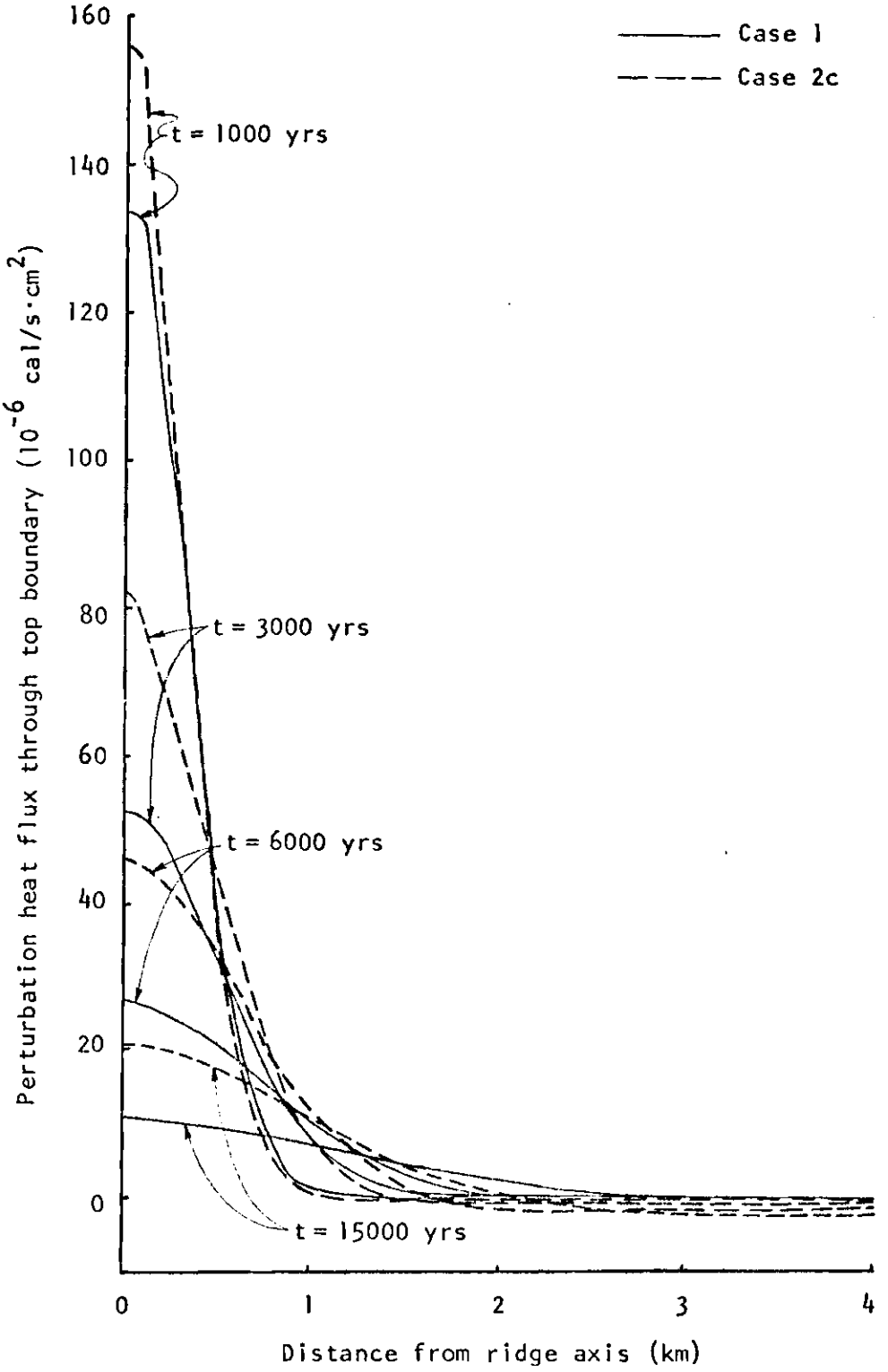

Figure 6. Comparison of Perturbation Heat Fluxes through Top Boundary for Conductive Case (Case 1) with Those for Typical Convective Case (Case 2c).

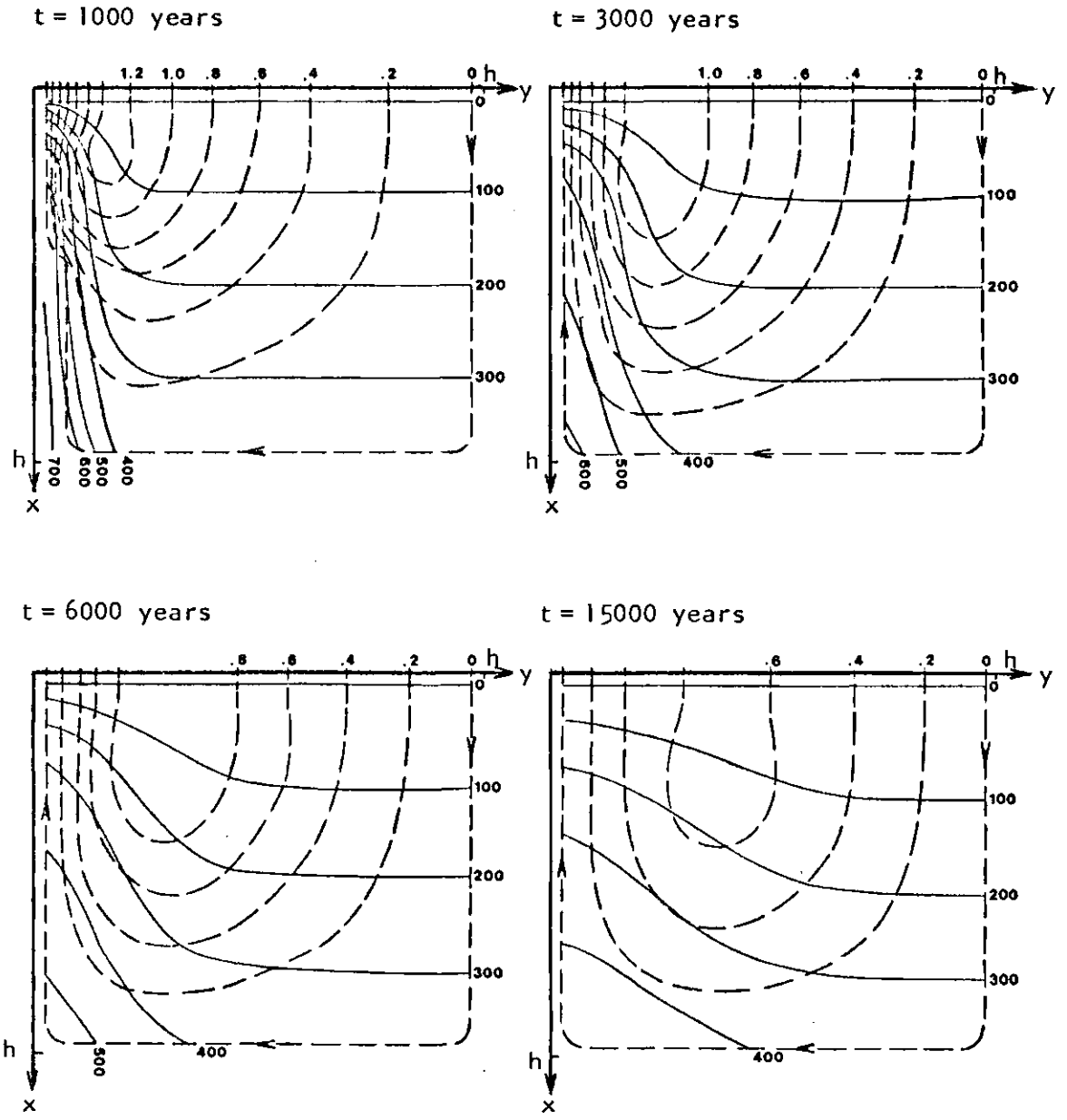

Figure 7. Typical Time Development of Hydrothermal Field (Case 2c).

the axis and down away from it. The center of circulation moves continuously down and away from the axis. Velocities are inversely proportional to streamline spacing [equations (25)]. Thus velocities are greatest at shallow depths near the axis and generally decrease with distance from the axis and depth. At a given point in space the velocity increases to a maximum and then decreases. Shallow points at the axis reach their maximums first (by the end of 1000 years), and deep points away from the axis last (by the end of 6000 years). The velocity distribution becomes more symmetric with increasing time.

Fluid circulation is induced by horizontal temperature gradients [equation (21)]. Such gradients result in differential expansion of fluid so that fluid density decreases in the direction of increasing temperature. The lighter fluid in the higher temperature regions tends to move up, and heavier fluid moves in to replace it. Thus fluid motion near the axis is up. The center of circulation moves in response to the changing horizontal temperature gradients. As these gradients increase down (as a result of horizontal convection toward the axis) and away from the axis (as a result of horizontal conduction from the axis), the center of cellular circulation follows. Maximum velocities occur when and where horizontal temperature gradients are maximum.

Figure 8 compares temperature fields for the convective case (solid lines) with those for the conductive case (dashed lines) at 6000 and 15000 years. Isotherms for the convective system are displaced in the direction of fluid motion, i.e., in the direction of convective heat transfer. The amount of displacement at a point is proportional to the time average of the product of the velocity and the temperature gradient at that point

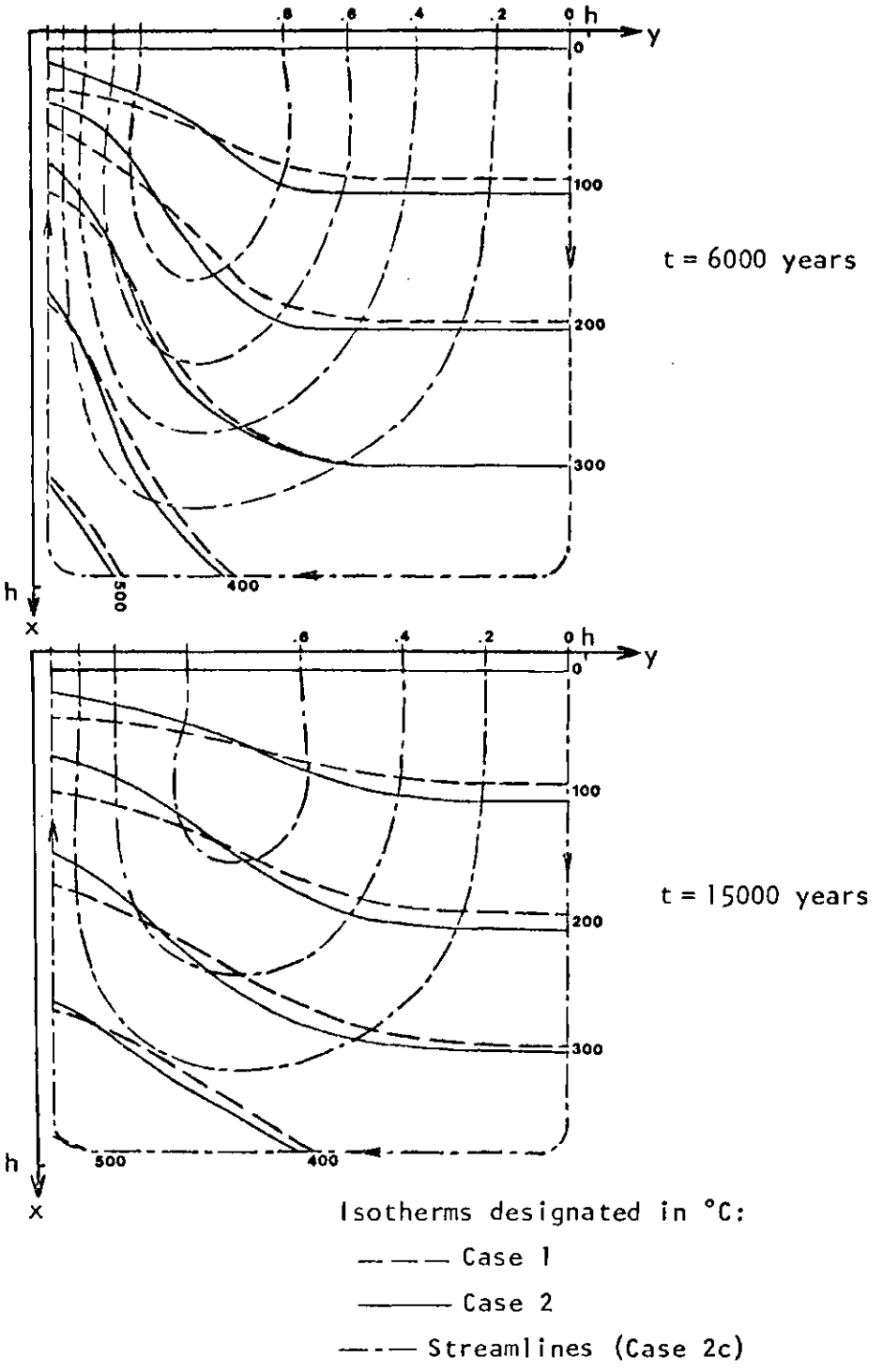

Figure 8. Comparison of Temperature Fields for Conductive Case (Case 1) with Those for Typical Convective Case (Case 2c).

[equation (20)].

The dashed curves of Figure 6 represent the perturbation surface heat fluxes, q''s, at various times for the convective system. General features of these curves are typical of all convective cases. Upflowing fluid near the axis has increased vertical temperature gradients near the surface relative to those for the conductive case, and thus q' is higher. Downflowing fluid away from the axis has decreased vertical gradients, and thus q' is lower. Negative perturbations occur where gradients have been reduced below the non-perturbation value, F. Temporal changes in q' at a point resemble those for the conductive case, but spatially, q' does not decrease monotonically with distance from the axis (as it does for the conductive case) until late in the cooling process. This non-monotonic decrease arises because of unevenness in the downward surface velocity distribution.

Figure 9 shows hydrothermal fields for three cases of homogeneous, isotropic permeability at t = 15000 years. All cases use different contour intervals in their streamline representation. A comparison of the streamline spacings for these intervals shows that velocities vary roughly according to 1.5K. Thus the degree of isotherm displacement increases with permeability. Isotherms are pushed closer to the ridge axis by greater horizontal velocities for cases of higher permeability, so that horizontal temperature gradients are more concentrated at the axis and centers of circulation remain closer to it. Isotherms are also displaced higher at the axis by greater vertical velocities, so that centers of circulation remain higher. For the case where K = 0.1, a horizontal temperature gradient increasing away from the axis was developed by a high

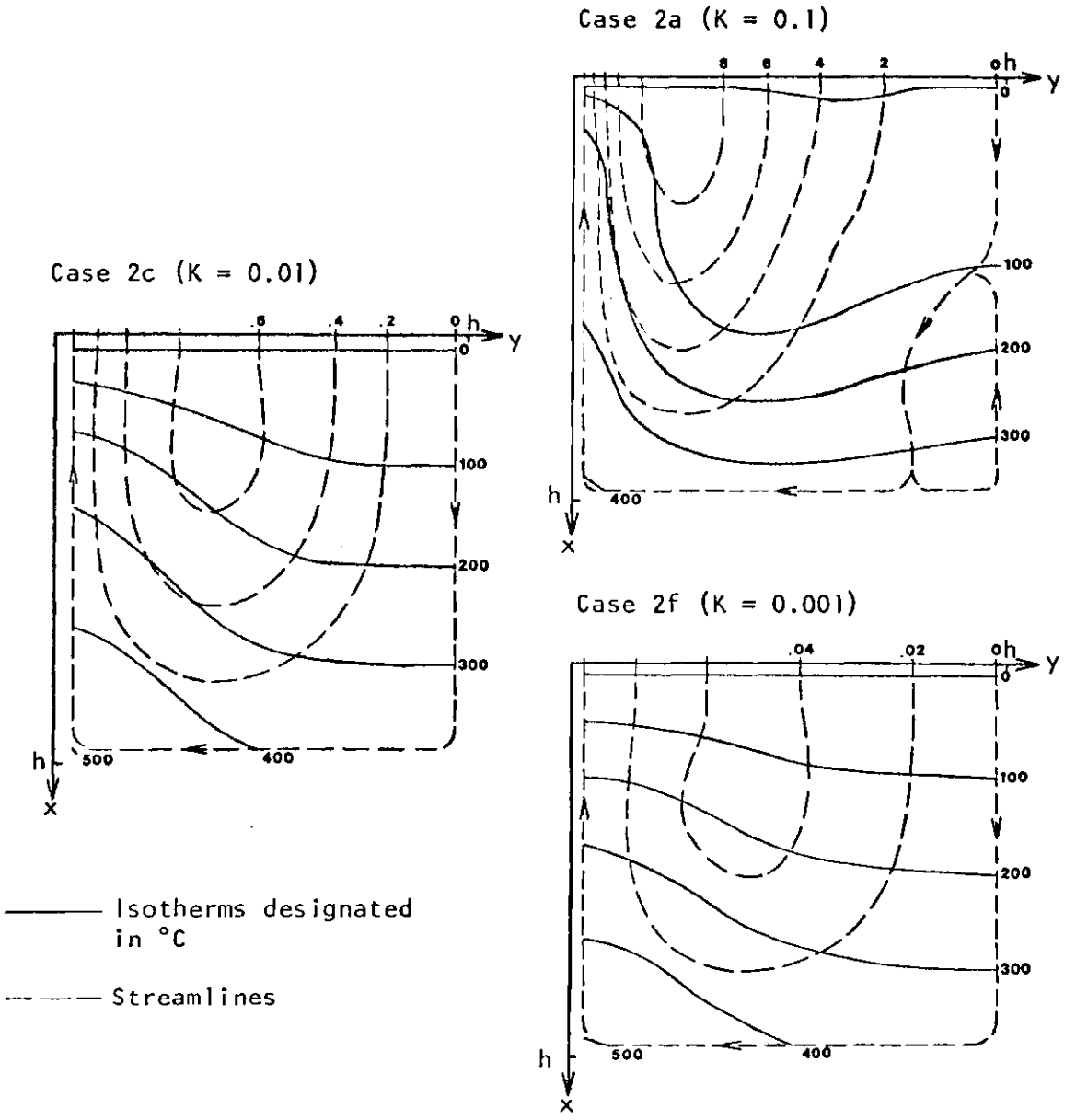

Figure 9. Hydrothermal Fields for Three Cases of Homogeneous, Isotropic Permeability at t = 15000 Years.

velocity gradient in the opposite direction. This temperature gradient has produced a second convection cell.

Figure 10 shows the hydrothermal fields at t = 15000 years for cases of homogeneous (case 2c: K = 0.01) and inhomogeneous (case 3: K linearly decreasing with depth from K_{max} = 0.01), isotropic permeability distributions. Velocities are everywhere greater for the homogeneous case, so that isotherm displacements are also greater. For the homogeneous case 50% of the fluid entering the system circulates to depths not greater than 2.9 km; for the inhomogeneous case 50% to depths not greater than 2.6 km. Flow in the inhomogeneous case thus tends to concentrate somewhat in the regions of higher permeability.

Figure 11 shows the hydrothermal fields at t = 15000 years for four thicknesses, d, of the permeable layer. Velocities, and therefore isotherm displacements, increase with d, and horizontal velocities tend more to increase with depth as d decreases. Cooling of the impermeable region increases with d (c.f. the maximum temperatures in the lower left corners). For lower values of d centers of circulation are higher and closer to the axis.

Figure 12 shows the hydrothermal fields at t = 15000 years for three cases of anisotropic permeability and one case of isotropic permeability. All cases have the same vertical permeability, K = 0.01. With decreasing horizontal permeability, velocities decrease, and centers of circulation move toward the axis.

Figure 13 shows the perturbation heat flux through the top boundary, q', at t = 15000 years for most cases modeled. Part (a) shows curves for various values of homogeneous, isotropic permeability, and part (b)

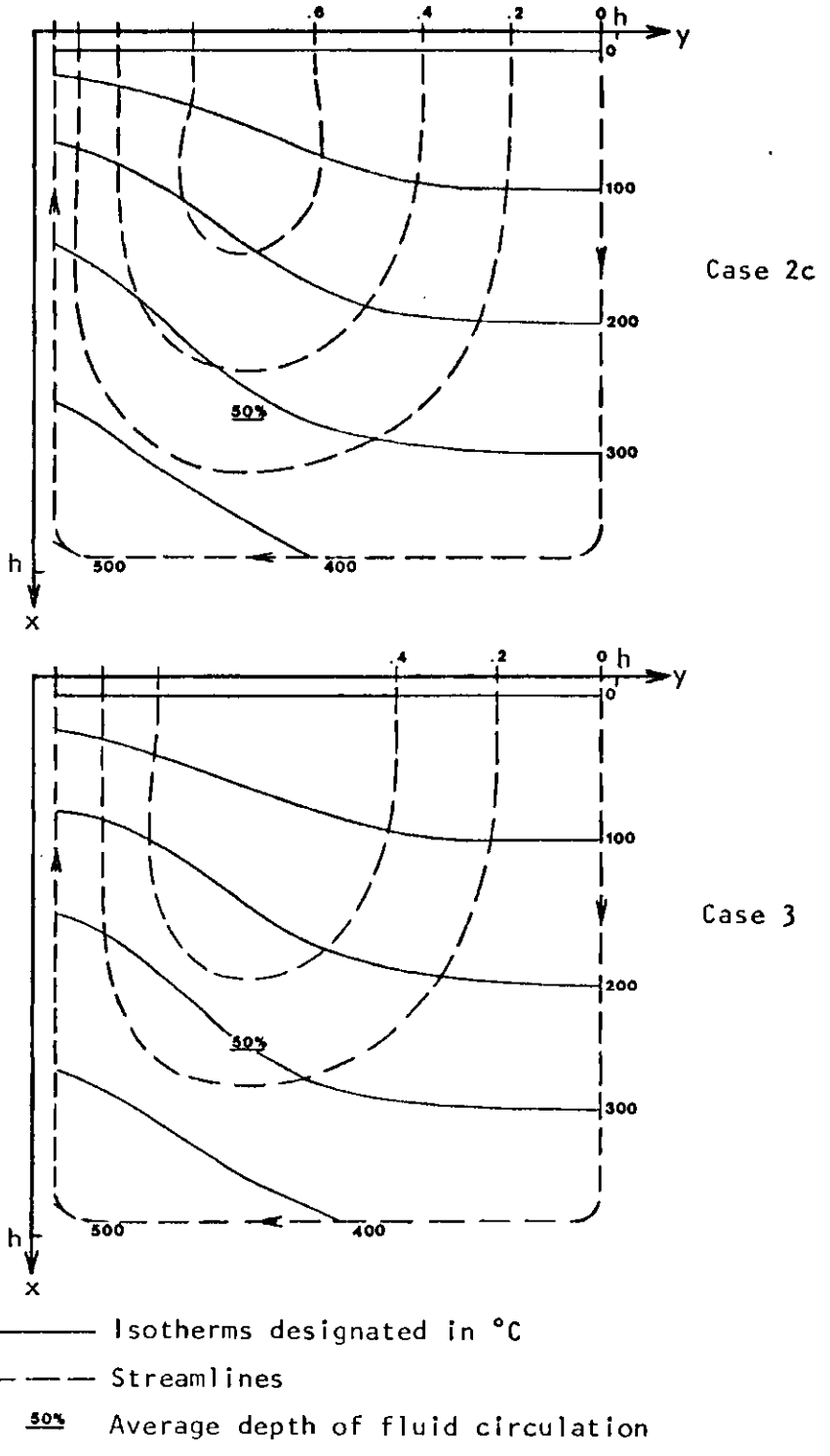

Figure 10. Hydrothermal Fields for Cases of Homogeneous (Case 2c) and Inhomogeneous (Case 3), Isotropic Permeability at t = 15000 Years.

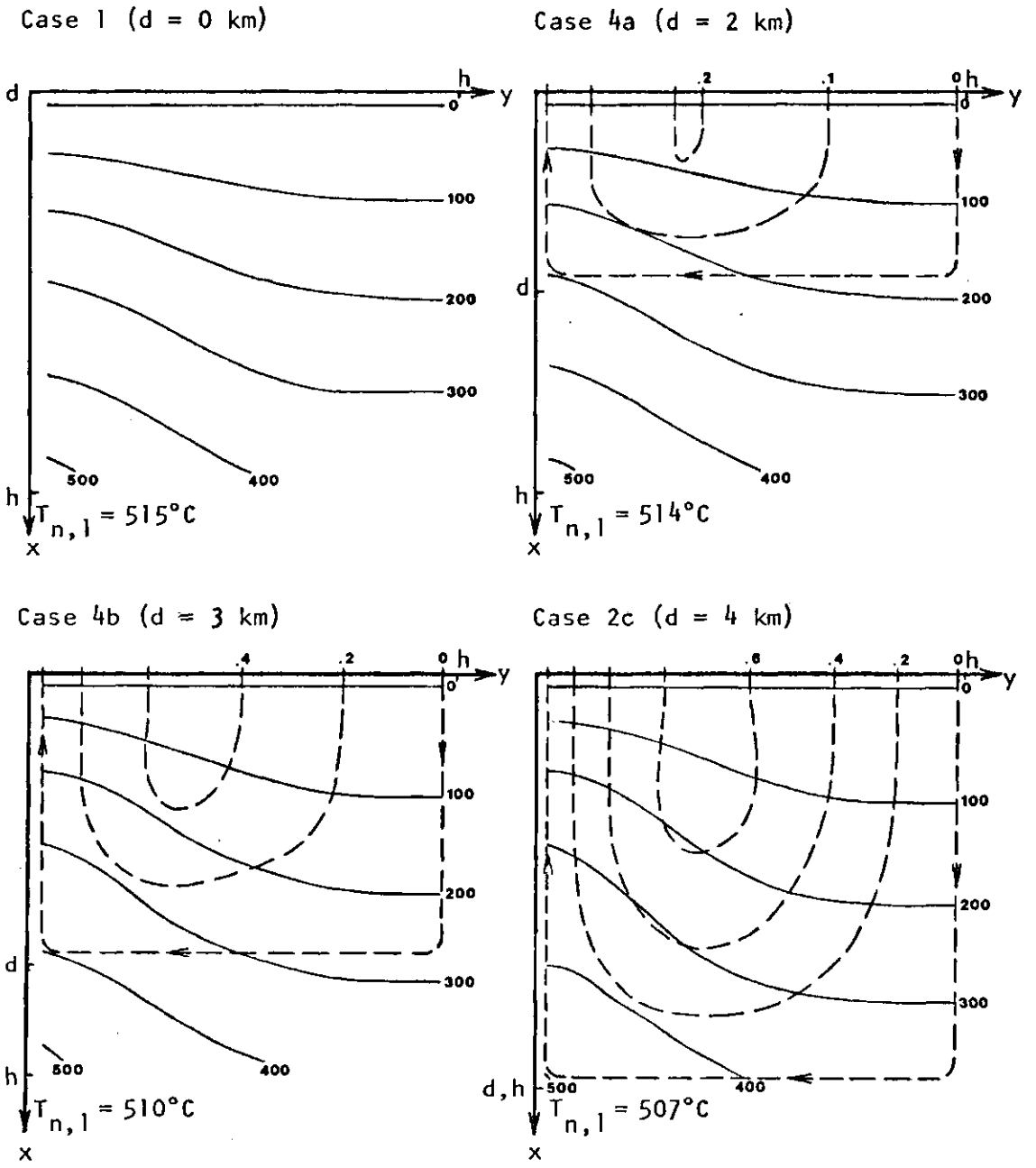

Figure 11. Hydrothermal Fields for Four Thicknesses of Permeable Layer at t = 15000 Years.

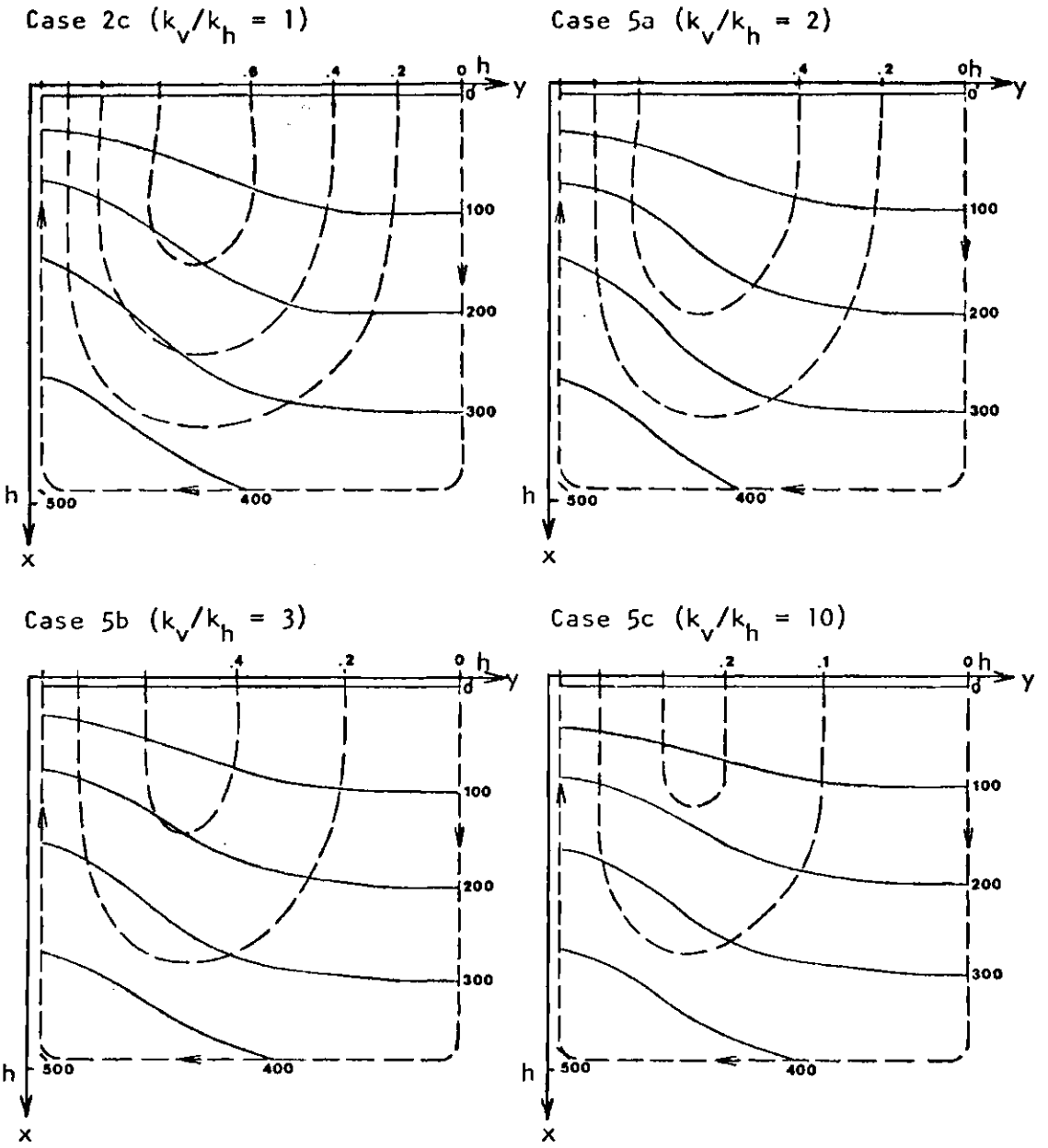

Figure 12. Hydrothermal Fields for Four Values of Horizontal Permeability at t = 15000 Years.

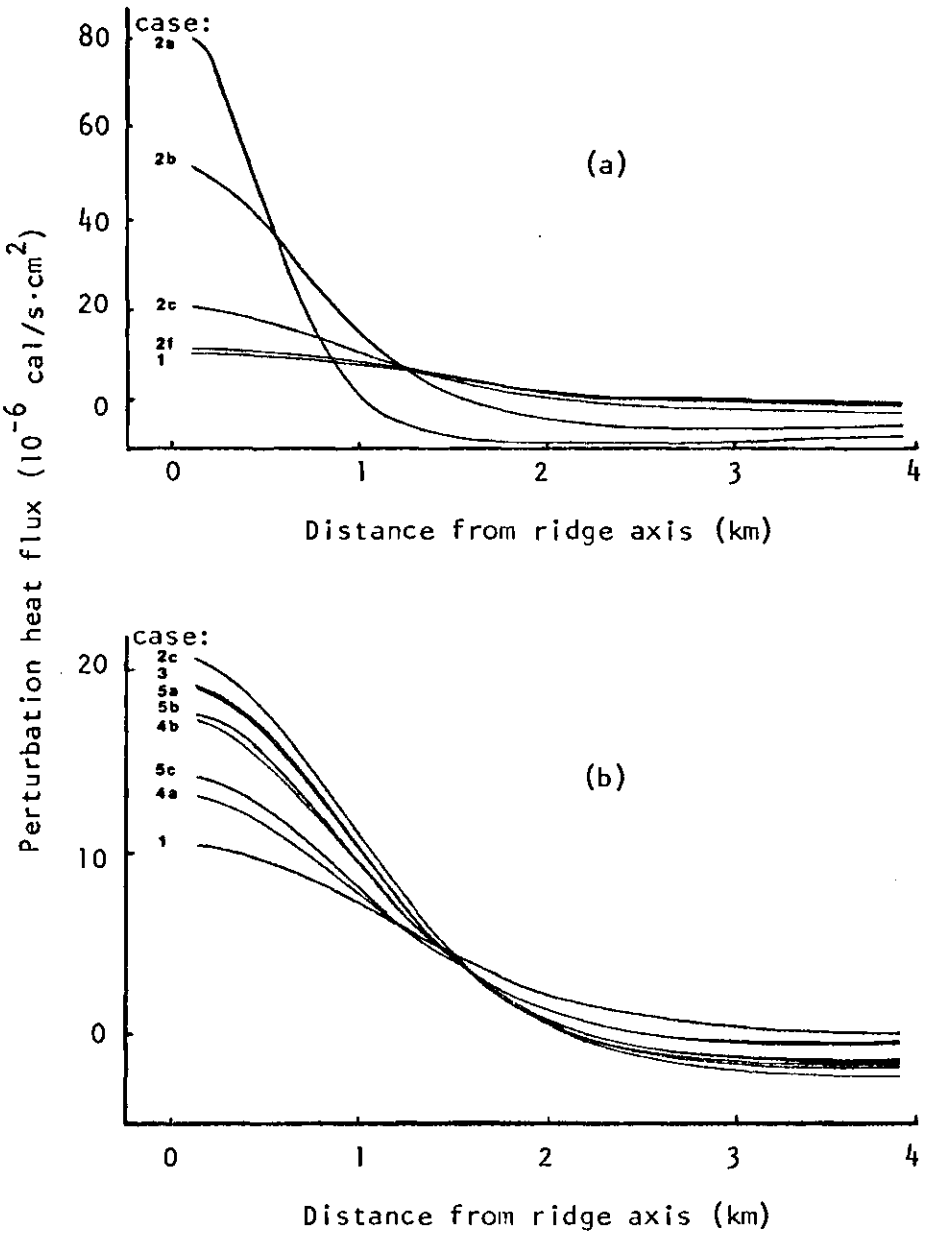

Figure 13. Perturbation Heat Flux through Top Boundary at t = 15000 Years.

includes those for other cases of permeability conditions. (Note that the vertical scales of the two graphs differ.) According to part (a), the higher the value of permeability, the higher the value of q' at the axis, the closer to the axis the intersection with the curve for the conductive case, and the greater the magnitudes of the negative perturbations away from the axis. The curves of part (b) for the other cases of permeability conditions intersect within a narrow range about 1.7 km from the ridge axis. Such a small region, where all these cases have the same vertical temperature gradient at the surface, exists since centers of circulation are close and velocities near these centers are low.

Curve (a) of Figure 14 represents the difference at t = 15000 years between total heat conducted out in convective cases 2b-f and total heat conducted out in conductive case 1 as a function of permeability, Q'(case 2) - Q'(case 1) [Q' from equation (35)]. For this range of permeability values, this function is linear. Curve (b) represents the total volume of fluid circulation, C, by t = 15000 years as a function of permeability for the same cases. This functional relationship is roughly linear also. Superimposed on each of these curves are the values of these functions for the other cases of permeability conditions.

Figure 15 shows total perturbation heat conducted out, Q', as a function of time for all cases. The total non-perturbation heat conducted out, Q^{o}, is also shown. For all cases the amount of heat conducted out during the first 1000 years differs little from that for the conductive case. Except for the anomalous curve for case 2a, this difference for cases of homogeneous, isotropic permeability appears to be linearly proportional to permeability at all times. (This was shown to be the case at t = 15000 years in Figure 14.) The slopes of all curves for

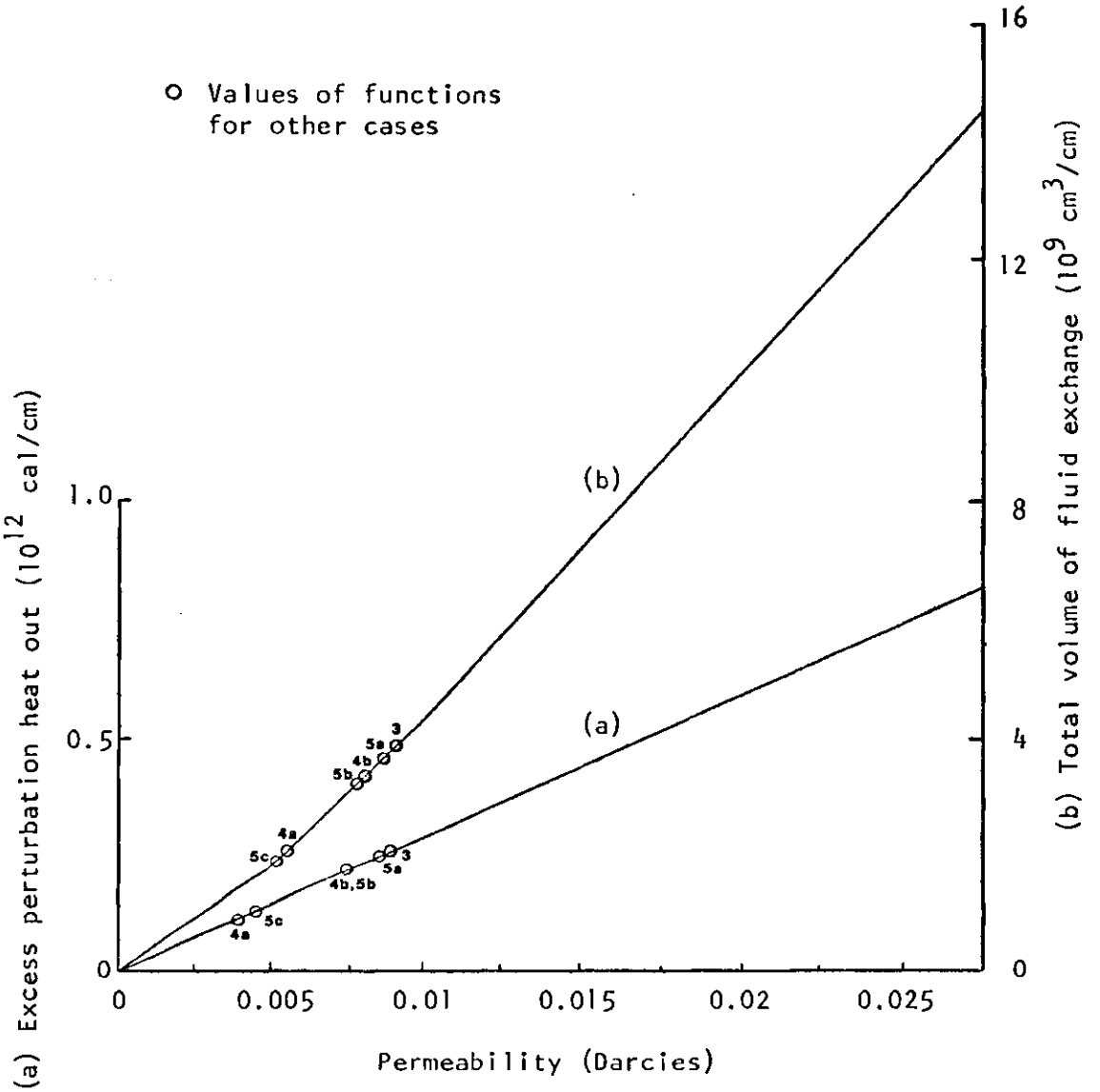

Figure 14. Perturbation Heat Conducted Out in Excess of That for Conductive Case and Total Volume of Fluid Exchange as Functions of Permeability for Cases 2b-f at t = 15000 Years.

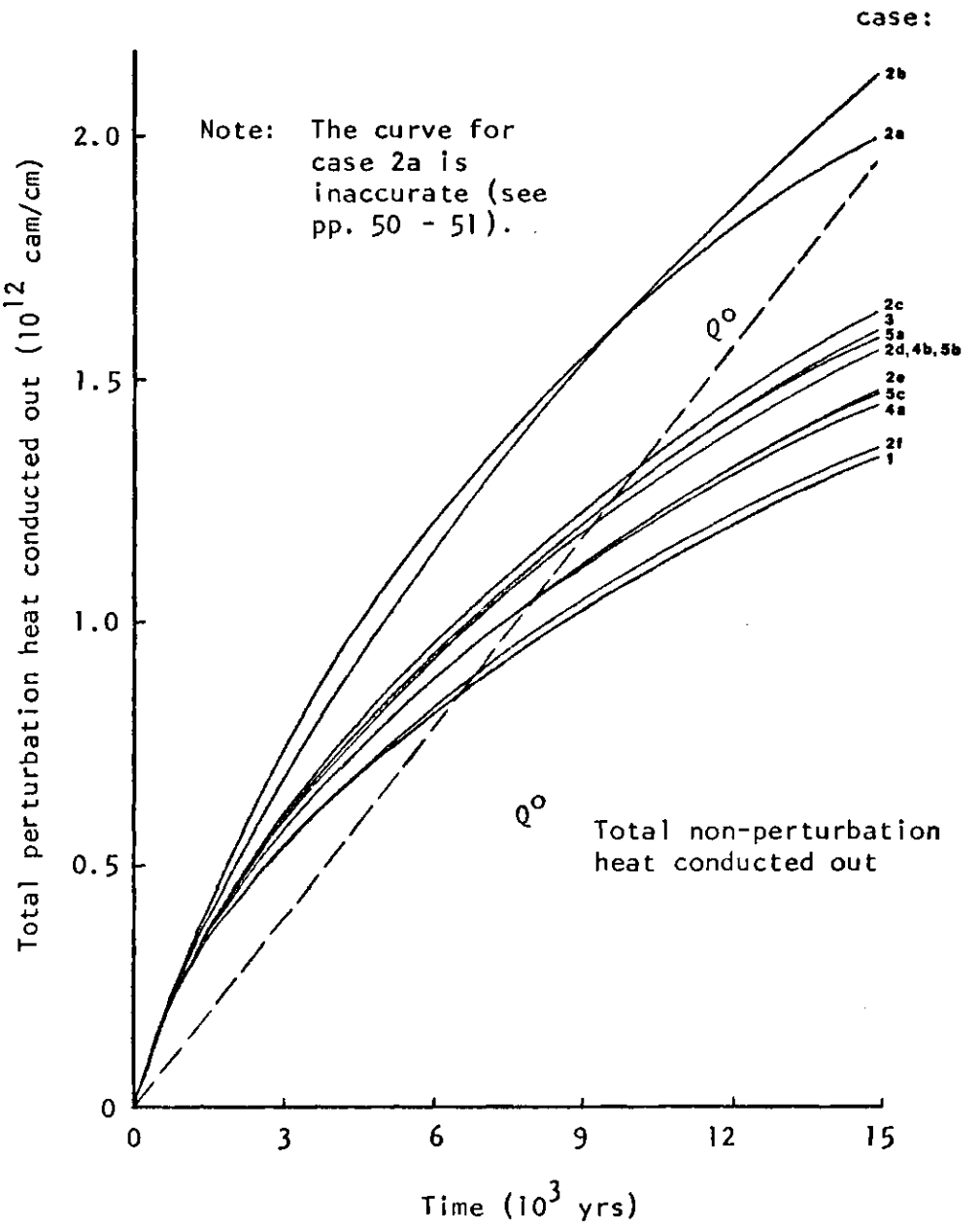

Figure 15. Total Perturbation Heat Conducted through Top Boundary as Function of Time.

convective cases are everywhere greater than those for the conductive case, indicating that the average heat flux over the surface of the model is always greater for convective cases. Only in the beginning of the cooling history are the slopes greater than that of the non-perturbation curve Q^{o}, indicating that the average perturbation heat flux is only then greater than the non-perturbation heat flux.

For inhomogeneous case 3 the average value of permeability over the whole model is slightly greater than 0.005. The Q' curve in Figure 15 for case 3, however, is well above that for case 2e (K = 0.005), and according to Figure 14, the amount of cooling for case 3 at the end of 15000 years is equivalent to that for a case of homogeneous permeability with K = 0.009. Permeabilities near the surface, therefore, are clearly more important than those at greater depths in determining the cooling history of the system. This is so because vertical flow (affecting vertical temperature gradients) is more concentrated near the surface. That depth of circulation is important, however, even when permeability decreases with depth, is evident by comparing the curve of Figure 15 for case 4a. In this case the average permeability over the model is also 0.005. While at depths less than 2 km, higher permeabilities occur than for case 3, depth of fluid circulation cannot exceed 2 km. From Figure 14 cooling for case 4a corresponds to that for a homogeneous permeability of 0.004 over the whole model, a much lower value.

The Q' curve in Figure 15 for anisotropic case 5a (p=2) is just slightly below that for case 3. If twice as much vertical as horizontal flow occurred (as appears to be true), an effective isotropic permeability could be determined from the formula: $K_{eff} = \frac{2K + K/p}{3}$. For

case 5a, $K_{eff} = 0.0083$; for anisotropic case 5b ($p = 3$), $K_{eff} = 0.0078$; and for anisotropic case 5c ($p = 10$), $K_{eff} = 0.007$. The effective isotropic permeabilities from Figure 14 for these cases are 0.0086, 0.0075, and 0.0045, respectively. Comparing these two sets of values, it appears that the relative importance of vertical fluid flow decreases with decreasing horizontal permeability.

For case 4b (d = 3 km) the average permeability over the model is 0.0075, and the curve in Figure 15 for case 4b is identical to that for case 2d (K = 0.0075). For case 4a (d = 2 km) the average permeability over the model is 0.005, but the curve in Figure 15 for case 4a lies below that for case 2e (K = 0.005). From Figure 16 the homogeneous permeability resulting in cooling of the system equivalent to that of case 4a is approximately 0.004, but a greater volume of fluid circulation was required by case 4a to produce this cooling effect [see curve (b)]. A greater volume of fluid circulation was also required by case 4b to produce the equivalent cooling effect of case 2d. Clearly, more efficient cooling systems are those of homogeneous, isotropic permeability.

By comparing curves (a) and (b) of Figure 14 some conclusions regarding the cooling efficiencies of the hydrothermal systems may be made. For cases of homogeneous, isotropic permeability, the ratio of the two functions [Q'(case 2) - Q'(case 1) and C] is roughly constant and equal to 70 cal/cm^3. Thus about 70 calories of heat, in excess of the amount when no circulation occurs, are conducted out of the model for every gram of water entering. For all cases where permeability conditions vary, this ratio is lower, but almost imperceptibly so for case 5a ($k_v/k_h = 2$). The magnitude of this quantity is certainly related to

average length of circulation path.

Figure 16 shows total volume of fluid exchange, V, as a function of time for all cases except 2a. This volume is roughly proportional to permeability for cases 2b-f. [This proportionality was shown in curve (b) of Figure 14 for t = 15000 years.] For all cases the rate of circulation (indicated by the inclination of the curves) increases gradually during the first thousand years, reaches a maximum within the next thousand years, and then decreases continuously.

Table 2 shows the sum of the perturbation heat conducted out [Q' from equation (35)] and the perturbation heat content of the system [Q' from equation (36)] at three times for all cases. The sums for the convective cases decrease with increasing time; the amount of decrease seems to increase with increasing fluid circulation (c.f. Figure 16). All sums should equal the original heat perturbation introduced by the intrusion, $5 \cdot 64 \cdot 10^{12}$ cal/cm, and discrepancies indicate that energy (heat) has not been conserved. The source of these discrepancies is discussed in the next chapter.

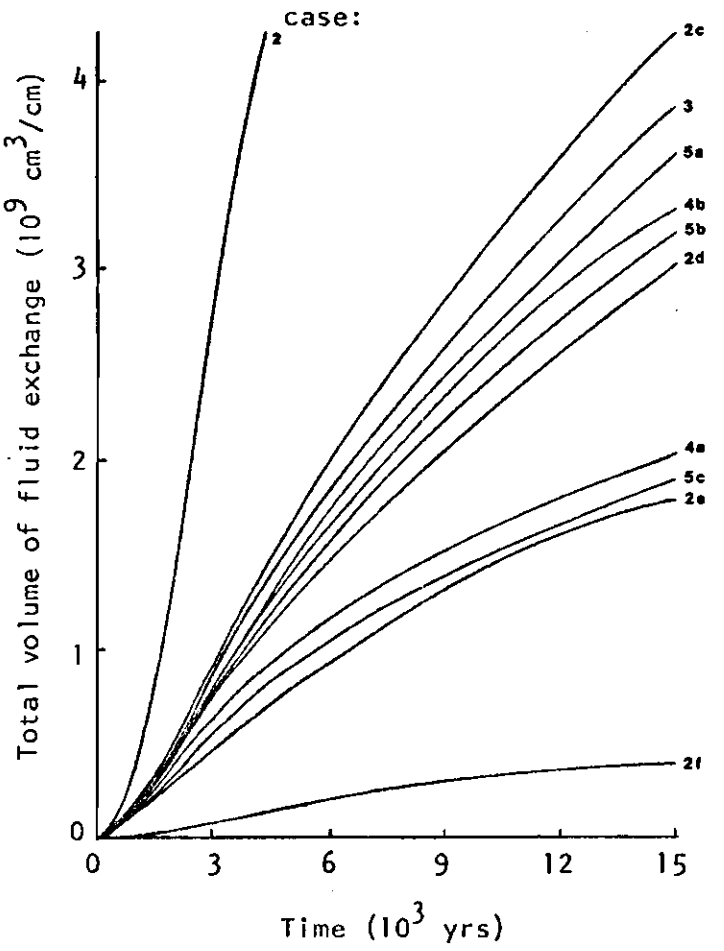

Figure 16. Total Volume of Fluid Exchange as Function of Time.

Table 2. Sum of Perturbation Heat Conducted Out and Perturbation Heat Content of System

0	Time (10^3 yrs)	3	6	15
5.64	Case			
	1	5.64	5.64	5.65
	2a	3.13	0.75	-3.01
	2b	5.23	4.80	3.98
	2c	5.56	5.48	5.37
	2d	5.58	5.54	5.47
	2e	5.61	5.58	5.54
	2f	5.63	5.63	5.62
	3	5.56	5.49	5.40
	4a	5.60	5.57	5.55
	4b	5.57	5.52	5.45
	5a	5.57	5.50	5.41
	5b	5.57	5.49	5.44
	5c	5.60	5.56	5.52

Note: Sums are in 10^{12} cal/cm.

CHAPTER VI

RELIABILITY OF RESULTS

The reliability of the results depends upon the degree of precision and accuracy in the solutions to the equations and the degree of correspondence of the model to reality.

Precision was limited by cumulative round off errors arising since numerical computations were carried out only to a finite number of significant figures. These errors, however, should have been small compared to those arising from the crudeness of the model. Accuracy was limited by truncation errors introduced when the differential equations were converted to algebraic representations (see footnote 3 on page 19). Generally, solution inaccuracies would have been on the order of ΔX or 5% (Torrance, 1968). The truncation error for the convection term of equation (20), however, included the quantities:

$$\frac{\Delta X |v_{x_{i,j}}|}{2} \frac{\partial^2 \theta_{i,j}}{\partial X^2} \quad \text{and} \quad \frac{\Delta Y |v_{y_{i,j}}|}{2} \frac{\partial^2 \theta_{i,j}}{\partial Y^2}$$

(Torrance, 1968), so that the temperature at every point was reduced by these amounts every computation step. When velocities were large, the magnitudes of these quantities became large and heat energy effectively disappeared from the system.

The degree of precision and accuracy in the solutions can be approximated through Table 2, where energy values for all times and cases

should equal $5 \cdot 64 \cdot 10^{12}$ cal/cm. For all except two cases, values differ from this by less than 5%. For cases 2a and 2b discrepancies were 31% and 153%, respectively; velocities were high, and therefore truncation errors were significant. These inaccuracies account for the anomalous behavior of the curve for case 2a in Figure 15. The curve for case 2b is probably also low, and all results for these cases must be interpreted with caution.

For no cases modeled was the original heat perturbation reduced by as much as 50% by the end of the 15000 year period. Because the reductions for convective cases were not considerably greater than that for the conductive case, average surface heat fluxes for the convective cases always exceeded average fluxes for the conductive case. Only a portion of the transient conditions building up to an equilibrium oscillatory state were modeled. For the range of permeabilities considered, modeling with periodic intrusions must be carried out for longer times in order to determine conditions closer to reality.

At least for cases modeled with $K > 0.0071$, conditions were such that Rayleigh convection would exist before the emplacement of the intrusion, i.e., the Rayleigh number for the system was greater than the critical value of 17.7 (Nield, 1968). (Rayleigh numbers have not been determined for cases of inhomogeneous or anisotropic permeability.) The size of the convection cells would therefore initially be set. For cases 4a and 4b ($d = 2$ km and $d = 3$ km) cells would not be oblong, as assumed here. Also, pre-intrusion velocities would not equal zero, as assumed. Since velocities reached their maximum values early, however, results for the 15000 year period probably were affected little by this assumption.

In the formulation of the equations it was assumed that perfect thermal contact would exist between the circulating fluid and the rock. Actual solution velocities were low enough that this assumption would seem to be valid. The maximum Darcy velocity reached was around $5 \cdot 10^{-6}$ cm/s (for case 2a) when K = 0.1. Actual velocities may be determined if crack widths and intercrack spacings are known. Assuming an intercrack spacing of 100 cm and using a formula given by Lister (1974) relating permeability to intercrack spacing gives 0.045 cm as the corresponding crack width. The actual fluid velocity through these cracks would be $\frac{100}{0.045} \times 5 \cdot 10^{-6}$ cm/s $\doteq$ 0.01 cm/s. All other solution velocities would lie below this value.

Since perfect thermal contact between fluid and rock was assumed, the additional assumption of a zero degree isothermal upper boundary precluded the possibility of any heat being convected out of the system. If the ocean had not been assumed to act as a perfect heat sink (maintaining the upper boundary at zero degrees), upon emplacement of the intrusion, the upper boundary would have been differentially heated and the zero degree isotherm would have been displaced upward. Heat would have convected across the boundary, and fluid flow would have tended to carry the zero degree isotherm up still further near the axis with increasing time. The conductive fluxes at the boundary would have been lowered from those for the zero degree boundary case since vertical temperature gradients would have been lowered. This situation probably would have produced results closer to reality than the situation of the zero degree boundary.

CHAPTER VII

CONCLUSIONS

Changes in permeability conditions from homogeneous, isotropic distributions did not alter flow patterns or cooling effects significantly, but produced effects roughly equivalent to those for cases of slightly lower values (relative to permeability to vertical flow at the surface) of homogeneous, isotropic permeability. For higher values of permeability than those considered in this study, changes in permeability conditions may be more important. Changes in permeability conditions also may be more important at distances from the ridge axis where low permeability sediments overlie the igneous layer. In such regions vertical velocities would not greatly predominate, and maximum velocities would not be so concentrated near the surface of the porous layer. Thus fluid flow fields would be more sensitive to changes in horizontal and subsurface permeability conditions. Close to the ridge axis, topographic variations may be more important than gross permeability conditions in determining circulation patterns.

Actual fluid velocities through the porous rock were low. For example, assuming an intercrack spacing of 100 cm, a high velocity for case 2c would be around 0.0075 cm/s. For such low velocities turbulence would not tend to erode fractures and thus to increase permeability. Also, for such low velocities perfect thermal contact probably would exist between the porous rock and the fluid. If the ocean bottom remains

approximately an isotherm, it is likely that very little heat convects from the system.

Convective rearrangement of isotherms for low values of permeability did not substantially increase the cooling rate of the system over that for the conductive case. For example, a permeability of 0.001 Darcies increased the rate by only 1.5% over the 15000 year period. Substantial increases occurred for higher values of permeability. For example, a permeability of 0.0275 Darcies increased the rate by at least 60%.

Excess heat conducted out in convective cases (cases 2b-f) over that in the conductive case (case 1) was directly proportional to permeability (see Figure 14). Thus, extrapolating the curve of Figure 14 to higher values of permeability lends to the prediction that convective systems with permeabilities greater than or equal to 0.15 Darcies could completely reduce the original heat perturbation within 15000 years. Convective systems with permeabilities less than 0.15 Darcies would not remove the entire perturbation within this period.

Consider the system (with values of permeability less than 0.15 Darcies) from the point of view of a much larger time scale. From this viewpoint, the system would not remove the perturbation heat as fast as it enters. Portions of this heat, therefore,would spread laterally away from the axis, out of the original model (disregarding the right temperature boundary condition). The amount of this heat would approach 0 as permeability approaches 0.15 Darcies. Superimposed on this large-scale system of laterally spreading heat would be the convective system that concentrates the surface heat flux at the ridge axis and depresses it

away from the axis. The higher the permeability of the model, the greater and narrower the concentration would be. Eventually the system would reach a "steady-state" degree of spread, and the rate of perturbation heat conduction through the surface of the system would equal the rate of heat intrusion at the axis. The total perturbation heat flux over the surface for all such systems would be the same, but the spatial distributions of the fluxes and the linear extents of the systems would vary with permeability.

Ocean-floor heat-flow measurements have been concentrated away from ridge axes, at distances where sediments are sufficiently thick to accommodate measuring instruments. Such a concentration of measurements over this model would result in a lower average value of flux being measured than the actual average value. The higher the permeability at the axis, the lower the average measured flux would be. It has been concluded that lower-than-expected measured values of ocean-floor heat flux indicate that much heat is being transmitted through the ocean floor by convection. According to this model, however, no heat need be convected through the ocean floor to account for the low average values measured.

CHAPTER VIII

RECOMMENDATIONS

The basic model may be modified for further meaningful study. A model may be developed of the quasi-steady-state system described in the last chapter by extending modeling to t >> 15000 years. The occurrence of periodic intrusions could easily be incorporated into the program, and the right temperature boundary condition could be modified to allow for heat transmission.

The model might also be modified so as to test the effects of irregular surface topography. Irregularities could be represented as non-uniform surface temperature and pressure distributions. Cases modeled could be general or could attempt to simulate actual characteristics at ridge axes [see Moore et al. (1974)].

To consider effects of larger values of permeability (greater than 0.0275 Darcies), the finite difference representation of the convection term would have to be made conservative. Even if this is done, however, the model would tend to break down as velocities increase since (1) flow would become turbulent and (2) perfect thermal contact would cease to exist. Approximate values of permeability where this breakdown would occur could be estimated from the results of this study.

The present model might be modified for study of the intrusion-fluid system on a smaller scale. The grid point density would be increased, while maintaining the grid point spacing sufficiently larger than any

realistic intercrack spacing. A more gradual temperature dependence of permeability based on thermo-elastic effects might be introduced. The results obtained would be of interest from a geochemical standpoint.

APPENDIX A

DETAILS OF FINITE DIFFERENCE SOLUTIONS

Stream Function

Boundary conditions for ψ in finite difference form are for the side and bottom boundaries:

$$\psi_{i,1} = \psi_{i,m} = \psi_{npp,j} = 0, \tag{39}$$

where i = 1,2,...,npp and j = 1,2,...,m, from equation (28) and for the top boundary:

$$\frac{\psi_{2,j} - \psi_{1,j}}{\Delta X} = 0,$$

where j = 1,2,...,m, from equation (27). Thus,

$$\psi_{1,j} = \psi_{2,j}. \tag{40}$$

Conditions when the convection cell is displaced out of regions where $\theta \geq \theta_r$ are discussed later in this section.

Inside the circulation boundaries, from equation (29),

$$\psi_{i,j} = \frac{1}{2(1+p)} \left[p\left(1 + \frac{A\Delta X}{2K_i}\right)\psi_{i-1,j} + p\left(1 - \frac{A\Delta X}{2K_i}\right)\psi_{i+1,j} + \psi_{i,j-1} + \psi_{i,j+1} + \frac{K_i \Delta X R}{2}\left(\theta_{i,j-1} - \theta_{i,j+1}\right)\right], \tag{41}$$

where $i = 2,3,\ldots,npp-1$ and $j = 2,3,\ldots,m-1$ and ΔY has been replaced by ΔX. Applying equation (41) at points (2,j), combining with equation (40), and rearranging gives:

$$\psi_{2,j} = \frac{1}{2(p+1)} \{1 - \frac{1}{2(p+1)} [p(1 + \frac{A\Delta X}{2K_2})]\}^{-1} [p(1 - \frac{A\Delta X}{2K_2})\psi_{3,j} + \psi_{2,j-1} + \psi_{2,j+1} + \frac{K_2 \Delta XR}{2} (\theta_{2,j-1} - \theta_{2,j+1})], \quad (42)$$

where $j = 2,3,\ldots,m-1$. Equation (42) will be applied at points where $i = 2$ and equation (41) at points where $i = 3,4,\ldots,npp-1$.

These equations will be solved by an iterative scanning technique called successive overrelaxation (Young, 1954). Applying this method to equation (41), the solution equation for $\psi_{i,j}$ is written:

$$\psi_{i,j}^{(s+1)} = (1 - w_{i,j})\psi_{i,j}^{(s)} + w_{i,j} \{\frac{1}{2(1+p)} [p(1 + \frac{A\Delta X}{2K_i})\psi_{i-1,j}^{(s+1)} + p(1 - \frac{A\Delta X}{2K_i})\psi_{i+1,j}^{(s)} + \psi_{i,j-1}^{(s+1)} + \psi_{i,j+1}^{(s)} + \frac{K_i \Delta XR}{2} (\theta_{i,j-1} - \theta_{i,j+1})]\}. \quad (43)$$

[The solution equation for $\psi_{2,j}$ is written analogously for equation (42).] The superscripts (s) and (s+1) designate values obtained after s and s+1 scans of the grid system, respectively. For a suitable choice of the relaxation coefficient, $w_{i,j}$ (see Appendix B), the solutions to equation (43) will approach those to equation (41) as s increases. When $\tau_\ell > 0$, $\psi_{i,j}^{(0)}$'s for the first scan of the grid system will be assigned the solution values of $\psi_{i,j}$ at $\tau_{\ell-1}$. When $\tau = 0$, $\psi_{i,j}^{(0)}$'s will be assigned an

arbitrary constant value.

In order to prevent the accumulation of errors in one corner of the grid network and thereby to increase the rate of convergence, successive scans will be in different directions (Elder, 1966). Equation (43) involves scanning from the upper left to lower right corner of the grid network. The next three iterations will involve scanning from the other three corners. [The equations for each of these iterations will have different pairs of adjacent (on the grid system) ψ's superscripted "(s+1)".] The analogous equations for $\psi_{2,j}^{(s+1)}$ will be solved in turn when scanning at points (2,j) occurs. The solutions will be considered to have converged sufficiently when:

$$\frac{\max_{i,j}|\psi_{i,j}^{(s+1)} - \psi_{i,j}^{(s)}|}{\max_{i,j}|\psi_{i,j}^{(s+1)}|} < 0.0005. \qquad (44)$$

Scanning will be stopped either when this condition is met or when $s = s_{max} = 25$, whichever comes first. In most cases scanning will be stopped when $s < 25$.

Convection cell boundaries must be displaced inward out of impermeable regions where $\theta \geq \theta_r$. Therefore, when $\theta \geq \theta_r$ at point (i,j), solutions for ψ at this and at adjacent points will be specified such that no fluid flows within and perpendicular to the incremental area surrounding (i,j), i.e., such that:

$$v_{x_{i,j}} = v_{y_{i,j}} = 0,$$

and

$$v_{x_{i-1,j}} = v_{x_{i+1,j}} = v_{y_{i,j-1}} = v_{y_{i,j+1}} = 0.$$

To obtain these velocity conditions from equations (30), it is necessary that:

$$\psi = 0 \text{ at points } (i,j), (i-1,j), (i-1,j+1), (i+1,j), (i+1,j+1), (i,j-1), (i-1,j-1), \text{ and } (i,j+1). \quad (45)$$

To include (45) as a "modified" boundary condition within the scanning equations [equation (43) and its counterparts], before iterative scanning begins at τ_ℓ, the grid network will be scanned for points where $\theta^\ell \geq \theta_r$. For all such points (i,j), $\psi^{(0)}$'s and w's corresponding to the array points of (45) will be assigned the value zero. Thereby the required fluid flow boundary conditions will be incorporated into the solution for ψ^ℓ.

Velocity

The finite difference velocity equations (30) may be applied at all grid points except those lying along the top and right boundaries. At the top boundary, equation (30b) cannot be applied to obtain $v_{y_{1,j}}$. Solutions along this boundary can be obtained, however, from equation (23) so that:

$$v_{y_{1,j}} = 0,$$

where $j = 1,2,\ldots,m$. At the right boundary, equation (30a) cannot be applied to obtain $v_{x_{i,j}}$. It will therefore be assumed that:

$$v_{x_{i,m}} = v_{x_{i,m-1}}, \tag{46}$$

where i = 1,2,...,npp. This assumption is based on a reversal in the direction of the Taylor series expansion for the finite difference representation of equation (25a) at points (i,m) (see footnote 3 on page 19). Errors in conservation of fluid mass arising from this assumption will be small since velocities at points (i,m-1) will be relatively small.

Temperature

Equation (31) describes the temperature field at all interior points of the grid network, i.e., $\theta_{i,j}$ for i = 2,3,...,n-1 and j = 2,3,...,m-1. Along the top boundary $\theta_{1,j}$ (j = 1,2,...,m) will remain constant at its initial value of zero. The finite difference equations for temperature along the other boundaries will be derived by modifying equation (31) slightly. The conduction terms of this equation, $\frac{\theta_{i+1,j} - 2\theta_{i,j} + \theta_{i-1,j}}{(\Delta X)^2}$ and $\frac{\theta_{i,j+1} - 2\theta_{i,j} + \theta_{i,j-1}}{(\Delta Y)^2}$, are rewritten in the form:

$$\frac{\theta_{i+1,j} - \theta_{i,j}}{(\Delta X)^2} + \frac{\theta_{i-1,j} - \theta_{i,j}}{(\Delta X)^2} + \frac{\theta_{i,j+1} - \theta_{i,j}}{(\Delta Y)^2} + \frac{\theta_{i,j-1} - \theta_{i,j}}{(\Delta Y)^2},$$

whereby the rate of heat conduction to a grid point (i,j) is shown to be dependent upon the temperature difference between it and the four surrounding points. Along the left boundary, no heat is conducted to or from the left [equation (22)], so the portion of the conduction term $\frac{\theta_{i,j-1} - \theta_{i,j}}{(\Delta Y)^2} = 0$. Also, along this boundary $v_{y_{i,1}} = 0$, so that the heat

flow equation at the left boundary is:

$$\frac{\theta_{i,1}^{\ell+1} - \theta_{i,1}^{\ell}}{\Delta\tau_{\ell}} = \frac{\theta_{i+1,1}^{\ell} - 2\theta_{i,1}^{\ell} + \theta_{i-1,1}^{\ell}}{(\Delta X)^2} + \frac{\theta_{i,2}^{\ell} - \theta_{i,1}^{\ell}}{(\Delta Y)^2}$$

$$- \left\{ \begin{array}{ll} v_{x_{i,1}}^{\ell} \dfrac{(\theta_{i,1}^{\ell} - \theta_{i-1,1}^{\ell})}{\Delta X} & \text{if } v_{x_{i,1}}^{\ell} > 0 \\ v_{x_{i,1}}^{\ell} \dfrac{(\theta_{i+1,1}^{\ell} - \theta_{i,1}^{\ell})}{\Delta X} & \text{if } v_{x_{i,1}}^{\ell} \leq 0 \end{array} \right\} - v_{x_{i,1}}^{\ell} \frac{\partial\theta^{o}}{\partial X}, \quad (47)$$

where $i = 2,3,\ldots,n-1$. Similarly, at the right boundary $\dfrac{\theta_{i,j+1} - \theta_{i,j}}{(\Delta Y)^2} = 0$ and $v_{y_{i,m}} = 0$, so that:

$$\frac{\theta_{i,m}^{\ell+1} - \theta_{i,m}^{\ell}}{\Delta\tau_{\ell}} = \frac{\theta_{i+1,m}^{\ell} - 2\theta_{i,m}^{\ell} + \theta_{i-1,m}^{\ell}}{(\Delta X)^2} + \frac{\theta_{i,m-1}^{\ell} - \theta_{i,m}^{\ell}}{(\Delta Y)^2}$$

$$- \left\{ \begin{array}{ll} v_{x_{i,m}}^{\ell} \dfrac{(\theta_{i,m}^{\ell} - \theta_{i-1,m}^{\ell})}{\Delta X} & \text{if } v_{x_{i,m}}^{\ell} > 0 \\ v_{x_{i,m}}^{\ell} \dfrac{(\theta_{i+1,m}^{\ell} - \theta_{i,m}^{\ell})}{\Delta X} & \text{if } v_{x_{i,m}}^{\ell} \leq 0 \end{array} \right\} - v_{x_{i,m}}^{\ell} \frac{\partial\theta^{o}}{\partial X}, \quad (48)$$

where $i = 2,3,\ldots,n-1$. Likewise, at the bottom boundary $\dfrac{\theta_{i+1,j} - \theta_{i,j}}{(\Delta X)^2} = 0$ and $v_{x_{n,j}} = 0$, so that:

$$\frac{\theta_{n,j}^{\ell+1} - \theta_{n,j}^{\ell}}{\Delta\tau_{\ell}} = \frac{\theta_{n-1,j}^{\ell} - \theta_{n,j}^{\ell}}{(\Delta X)^2} + \frac{\theta_{n,j+1}^{\ell} - 2\theta_{n,j}^{\ell} + \theta_{n,j-1}^{\ell}}{(\Delta Y)^2}$$

$$- \begin{cases} v_{y_{n,j}}^{\ell} \dfrac{(\theta_{n,j}^{\ell} - \theta_{n,j-1}^{\ell})}{\Delta Y} & \text{if } v_{y_{n,j}} > 0 \\ v_{y_{n,j}}^{\ell} \dfrac{(\theta_{n,j+1}^{\ell} - \theta_{n,j}^{\ell})}{\Delta Y} & \text{if } v_{y_{n,j}} \leq 0 \end{cases}, \tag{49}$$

where $j = 2,3,\ldots,m-1$. Each of the two bottom corner points lies along two boundaries, and its equation involves the conditions for both of these boundaries. For the left bottom point,

$$\frac{\theta_{n,1} - \theta_{n,1}}{\Delta\tau_{\ell}} = \frac{\theta_{n-1,1}^{\ell} - \theta_{n,1}^{\ell}}{(\Delta X)^2} + \frac{\theta_{n,2}^{\ell} - \theta_{n,1}^{\ell}}{(\Delta Y)^2}; \tag{50}$$

and for the right bottom point,

$$\frac{\theta_{n,m}^{\ell+1} - \theta_{n,m}^{\ell}}{\Delta\tau_{\ell}} = \frac{\theta_{n-1,m}^{\ell} - \theta_{n,m}^{\ell}}{(\Delta X)^2} + \frac{\theta_{n,m-1}^{\ell} - \theta_{n,m}^{\ell}}{(\Delta Y)^2}. \tag{51}$$

APPENDIX B

DETERMINATION OF RELAXATION COEFFICIENT

Equation (29) applied at all interior grid points may be represented as the system of (n-2)x(m-2) equations:

$$\sum_{r=1}^{(n-2)(m-2)} a_{k,r}\psi_r + d_k = 0,$$

where the two-dimensional array in i and j is replaced by a one-dimensional array in r. Successive overrelation solution equations corresponding to equation (43) then are written:

$$\psi_k^{(s+1)} = (1 - w_r)\psi_k^{(s)} + w_r\left(\sum_{r=1}^{k-1} b_{k,r}\psi_r^{(s+1)} \sum_{r=k+1}^{(n-2)(m-2)} b_{k,r}\psi_r^{(s)} + c_k\right), \quad (52)$$

where $b_{k,r} = \begin{cases} -a_{k,r}/a_{k,k} & \text{if } k \neq r \\ 0 & \text{if } k = r \end{cases}$ and $c_k = -d_k/a_{kk}$ (Young, 1954).

According to Young (1954), the relaxation coefficient effecting the optimum rate of convergence is given by:

$$w_r = 1 + \left[\frac{\bar{\mu}}{1 + (1 - \bar{\mu}^2)^{1/2}}\right]^2, \quad (53)$$

where $\bar{\mu}$ is the spectral norm of the matrix $B = (b_{k,r})$. If $\bar{\mu}$ is overestimated in determining w_r, the effect on the rate of convergence of (52) will be small (Young, 1954). Since $\bar{\mu}$ is not easily determinable,

an overestimated value for it, $\bar{\mu}'$, will be found by means of the comparison theorem:

> If $b'_{k,r} > b_{k,r}$ for k and r = 1,2,...,(n-1)(m-1), then the spectral norm of B does not exceed that of B', i.e., $\bar{\mu} \leq \bar{\mu}'$ (Oldenburger, 1940).

The spectral norm, $\bar{\mu}'$, corresponding to the system of equations:

$$\psi'_{i,j} = \frac{1}{2(E^2 + F^2)} (E^2\psi'_{i-1,j} + E^2\psi'_{i+1,j} + F^2\psi'_{i,j-1} + F^2\psi'_{i,j+1} + c'_{i,j}) \qquad (54)$$

may be derived through methods given by Young (1954) to be:

$$\bar{\mu}' = 1/2(\cos \pi\Delta XE + \cos \pi\Delta XF). \qquad (55)$$

The values of E and F will be chosen so that each element $b'_{k,r}$ of matrix B' exceeds the corresponding element $b_{k,r}$ of matrix B. Thus the coefficients of equation (54) will be chosen so as to exceed the corresponding coefficients of equations (41) and (42). $\frac{E^2}{2(E^2 + F^2)}$ will be chosen to exceed slightly the largest of the coefficients of $\psi_{i-1,j}$ and $\psi_{i+1,j}$ from equation (41) and $\psi_{3,j}$ from equation (42); $\frac{F^2}{(E^2 + F^2)}$ will be chosen to exceed slightly the largest of the coefficients of $\psi_{i,j-1}$ and $\psi_{i,j+1}$ from equation (41) and $\psi_{2,j-1}$ and $\psi_{2,j+1}$ from equation (42). The overestimated value of $\bar{\mu}$ then will be obtained from equation (55), and w_r will be computed by substituting this value, $\bar{\mu}'$, into equation (53).

APPENDIX C

PROGRAMMING

The basic program applied to case 3 is reproduced on pages 73 through 77. For other cases the appropriate values of NPP = npp (line 9), PXY = p (line 19), PMAX = $K_{i=1}$ (line 20), and DKDX = $\frac{\partial K_i}{\partial X}$ (line 21) were changed. Minor changes in the velocity and stream function FORMATS (lines 309, 313, and 314) were also required for some cases of different permeability values. Print-outs were obtained at t = 1-,2-,3-,6-,9-,12-, and 15000 years. The average execution time for all cases was approximately 40 seconds.

Program Explanation

The DIMENSION statement reserves computer storage space for the following arrays:

T(I,J) = $\theta^{\ell}_{i,j}$

TNEW(I,J) = $\theta^{\ell+1}_{i,j}$

P(I) = K^{ℓ}_{i}

PSI(I,J) = $\psi^{\ell}_{i,j}$

U(I,J) = $v^{\ell}_{x_{i,j}}$

V(I,J) = $v^{\ell}_{y_{i,j}}$

Q(J) = $\frac{q'_j(t^{\ell+1})}{10^{-6}}$

$NT(I,J) = T^{\ell+1}_{i,j}$

$NU(I,j) = \dfrac{u^{\ell}_{x_{i,j}}}{10^{-8}}$

$NV(I,J) = \dfrac{u^{\ell}_{y_{i,j}}}{10^{-8}}$

$ABM(I) = p(1 - \dfrac{A\Delta X}{2K_i})$

$ABP(I) = p(1 + \dfrac{A\Delta X}{2K_i})$

$ABT(I) = \dfrac{K_i \Delta XR}{2}$

$TB(I) = \theta^{o}_{i,j}$

$TWPP(I,J) = \dfrac{w_{i,j}}{2(p+1)}$

$WPPD(J) = \dfrac{w_{2,j}}{2(p+1)} \{1 - \dfrac{1}{2(p+1)} [p(1 + \dfrac{A\Delta X}{2K_2})]\}^{-1}$

CONSTANTS AND VARIABLES defines constants and sets initial values of some variables:

M = m

N = n

NPP = npp

MD = DD/ΔX (width of intrusion in grid points)

ND = DD/ΔX (depth to intrusion in grid points)

DELX = ΔX

DELY = ΔY

DEPTH = h

TO = T_o

TOP = θ_r

TTT = $\theta^o(1,Y) = \frac{\partial \theta^o}{\partial X}$

HOT = $\frac{T_o \rho c h^2}{10^{12}}$

HT = $\frac{T_o \kappa}{\Delta X h \cdot 10^{-6}}$

PXY = p

PMAX = $K_{i=1}$

DKDX = $\frac{\partial K_i}{\partial X} = A$

RY = R

ITMAX = s_{max}

TH1 = τ for t = 1000 years

TH3 = τ for t = 3000 years

THG3 = τ for 3000 < t < 4000 years

NPRI is total number of print-outs

PRINT will be assigned the value "1" if $\tau_{\ell+1}$ corresponds to t = 1-,2-,3-6-,9-,12- or 15000 years

TIME = $\left\{ \begin{matrix} \tau_\ell & \text{(to line 206)} \\ \tau_{\ell+1} & \text{(from line 207)} \end{matrix} \right\}$ - τ (at last print-out)

TIM = τ_ℓ(to line 206) and $\tau_{\ell+1}$ (from line 207)

QQT = $\sum_{r=1}^{\ell+1} \sum_{j=1}^{m} \theta_{2,j}^{r} \Delta\tau_r$

D is $|\vec{v}_{max}|$ occurring since last print-out

NCNT = ℓ-1 (number of time steps)

DOWT = $V(t^{\ell})$ - V(t at last print-out)

TDOWN = $V(t^{\ell})$

ZERO VELOCITIES assigns zero to those components of $\overline{v}$ along the boundaries that remain constant at zero [equation (16)].

INITIAL TEMPERATURE FIELD AND PERMEABILITY FUNCTIONS defines $\theta^{1}_{i,j}$ [equation (33)] (lines 40-46) and stores the appropriate values in the arrays ABP(I), ABM(I), and ABT(I) [equations (41) and (42)] (lines 47-53).

BOUNDARY CONDITIONS FOR STREAM FUNCTION sets boundary conditions for ψ according to equation (39).

INITIAL STREAM FUNCTION GUESS assigns a value to all $\psi^{(0)}$'s to be used in the first solution equation for ψ^{1} [equation (43)].

RELAXATION COEFFICIENT computes the value of w_r as discussed in Appendix B. Line 73 corresponds to equation (55) with ACOS = $\overline{\mu}'$, and line 74 to equation (53) with W = w_r.

STREAM FUNCTION computes ψ^{ℓ} as discussed in Appendix A. Lines 79 to 96 locate points (i,j) where $\theta \geq \theta_r$ and for each such point set ψ and w equal to zero at the points specified in condition (45). Lines 100 and 101 cause successive changes in the direction of scan in the solution for ψ. Line 101 transfers control successively to four different statements by means of the value of ITERS. Each of these four statements begins a single scanning computation of ψ. Equation (44) is tested after each scan (lines 119, 138, 158, and 180). If equation (44) is satisfied, control is transferred out of the scanning loops to line 181. If equation (44) is not satisfied, control goes to line 97. If ITER = s_{max}, line 98

transfers control to line 181. Lines 181 and 182 compute $\psi_{1,j}$ according to equation (40).

VELOCITIES, TIME INTERVAL, AND PRINT-OUT CONTROL computes $\overline{v}^{\ell}$ in lines 185 to 195. Line 187 corresponds to equation (30a), 188 to (46), and 195 to (30b). Lines 196 to 206 define the value of DELTAU ($\Delta\tau_{\ell}$) as .9 the allowable value for stability [equation (32)]. Also, D = $|\overline{v}_{max}|$ is determined. Lines 207 to 216 cause print-outs to occur at $\tau_{\ell+1}$'s corresponding to t = 1-,2-,3-,6-,9-,12-, and 15000 years, redefining $\Delta\tau_{\ell}$ for computation steps just before print-out so that print-out occurs exactly at these times.

TEMPERATURES computes $\theta^{\ell+1}$ in lines 220 to 245. Line 223 corresponds to equation (50), 224 to (51), 228 and 229 to (47), 232 and 233 to (48), 239 and 240 to (31), and 244 and 245 to (49). Lines 251 through 253 store the values of $\theta^{\ell+1}$ in θ^{ℓ} for the next computation step. Lines 246 to 250 compute QQT = $\sum_{r=1}^{\ell+1} \sum_{j=1}^{m} \theta_{2,j}^{r} \Delta\tau_{r}$ to be used in computing Q' [equation (35)].

AMOUNT OF CIRCULATION computes DOWN = $\frac{1}{2} \sum_{j=1}^{m} v_{1,j}^{\ell}$ to be used in computing C [equation (37)] and DOWT = DOWT (at $t^{\ell-1}$) + $\frac{h^2 \rho c}{\kappa} C(t^{\ell})\Delta\tau_{\ell}$ to be used in computing V [equation (38)]. If $\tau_{\ell+1}$ is such that print-out will not occur, line 264 returns control to line 78 to compute $\psi^{\ell+1}$. Lines 265 to the end of the program are executed only when print-out will occur. Line 265 computes TDOWN = $V(t^{\ell})$. Line 266 computes CDOWN = $C(t^{\ell})$.

TOTAL HEAT computes SUMTT = $\frac{Q'(t^{\ell+1})}{10^{12}}$ [from equation (36)].

DIMENSIONS adds dimensions according to equations (18). Line 278

converts $\tau_{\ell+1}$ to $t^{\ell+1}$; lines 280 to 283 convert $\theta^{\ell+1} + \theta^{o}$ to $T^{\ell+1}$; and lines 284 to 288 convert v^{ℓ} to $\frac{u^{\ell}}{10^{-8}}$ and v^{ℓ}_{max} to $\frac{u^{\ell}_{max}}{10^{-8}}$.

HEAT OUT computes OHEAT = $\frac{Q'(t^{\ell+1})}{10^{12}}$ [from equation (35)].

CONDUCTIVE HEAT FLOW computes $\frac{q'_j(t^{\ell+1})}{10^{-6}}$ [equation (34)].

TIMES causes computation to stop when $t^{\ell+1}$ = 15000 years.

Print-Out Explanation

The print-out for case 3 at $t^{\ell+1}$ = 1000 years is shown on pages 78 through 80. Function labels have been added to the print-out titles.

Program Listing

```
      PROGRAM DYKE (INPUT,OUTPUT,TAPE5=INPUT,TAPE6=OUTPUT)
      DIMENSION T(20,20),TH(20),V(20,20),P(20),PSI(20,20),U(20,20),
     + V(20,20),B(20),N1(20,20),NU(20,20),NV(20,20),ABM(20),ABP(20),
     + ABT(20),TB(20),TMP(19,19),WPPB(19)
C
C CONSTANTS AND VARIABLES
      M=20 $ MM=M-1 $ M1=M+1
      FN=N=20 $ FNL=NL=N-1
      NPP=N
      NZ=NPP-2 $ NA=NPP-1 $ FNP=NPPP=NPP+1
      MD=1 $ ND=2
      DELX=DELY=1./FN $ SDELX=DELX**2
      DEPTH=4.E5
      TO=1200.
      TOP=690./TO
      TTT=400./TO
      HOT=TO*.12 $ HOTT=HOT/400.
      HT=TO*.01/(DELX*DEPTH*10.**(-6))
      PXY=1.
      PMAX=.01
      DKDX=-1.*FN/FNP*PMAX
      RY=6.1904*TO
      ITMAX=25
      TH1=.00263 $ TH3=.00789
      THG3=.01
      NPRI=PRINT=TIME=TIM=QOT=D=NCNT=0
      DOWT=TDOWN=0.
C
      WRITE(6,1111) TO,DELX,PMAX,PXY,DKDX
1111  FORMAT (///* DYKE TEMP = *F5.0*   DELX = *F4.3*   MAX*
     + * PERM = *F5.3/* XPERM/YPERM = *F3.1*   BPERM/DX = *F6.2///)
C
C ZERO VELOCITIES
      DO 47 I=2,NPP
47    V(I,1)=V(I,M)=0.
      DO 45 J=1,M
45    V(1,J)=U(NPP,J)=0.
C
C INITIAL TEMPERATURE FIELD AND PERMEABILITY FUNCTIONS
      DO 315 I=1,N
      FI=I $ FIN=FI-1. $ TB(I)=TTT*DELX*FIN
      DO 315 J=1,M
315   T(I,J)=0.
      DO 2 J=1,MD
      DO 2 I=ND,N
2     T(I,J)=1.-TB(I)
      PX=DELX*DKDX/2. $ PT=DELX*RY/2.
      P(1)=PMAX
      DO 1 I=2,NPP $ FFN=NPPP-I
      P(1)=PMAX*FFN/NPP
      ABP(1)=PXY*(1.+PX/P(I))
      ABM(I)=PXY*(1.-PX/P(I))
1     ABT(1)=PI*P(I)
C
C BOUNDARY CONDITIONS FOR STREAM FUNCTION
      DO 5 J=1,M
5     PSI(NPP,J)=0.
      DO 6 I=1,NA
6     PSI(I,1)=PSI(I,M)=0.
C
C INITIAL STREAM FUNCTION GUESS
      DO 250 I=1,NA
      DO 250 J=2,MM
250   PSI(I,J)=.1
C
C RELAXATION COEFFICIENT
      PP=1./(2.*(PXY+1.))
      Z=2.*PP*ABM(NPP)/(1.-2.*PP*ABM(NPP))
      Y=2.*PP*ABM(2)/(1.-PP*ABP(2)-2.*PP*ABM(2))
      IF(Z.GT.Y) Y=Z
      X=(1.-PP*ABP(2)-2.*PP)/(2.*PP)
      A=SQRT((X+Y)/2.)
      ACOS=(COS(3.142*DELX*A)+COS(3.142*DELY))/2.
      W=1.+(ACOS/(1.+SQRT(1.-ACOS**2)))**2
```

Program Listing (cont.)

```
      C
      C STREAM FUNCTION
            WPP=U*PP $ WM=1.-W
      18    ITERS=ITER=0
            DO 4 I=2,NA
            DO 4 J=2,MM
      4     TWPP(I,J)=WPP
            DO 7 I=2,NA
            IF((TB(1)+T(I,1)).GE.TOP) PSI(I-1,2)=PSI(I,2)=TWPP
           + (I-1,2)=TWPP(I,2)=0.
            DO 7 J=2,MM
            IF((TB(I)+T(I,J)).GE.TOP) PSI(I-1,J-1)=PSI(I-1,J)=PSI(I-1,J+1)
           + =PSI(I,J-1)=PSI(I,J)=PSI(I,J+1)=PSI(I+1,J)=PSI(
           + I+1,J+1)=TWPP(I-1,J-1)=TWPP(I-1,J)=TWPP(I-1,J+1)=TWPP(I,J-1)
           + =TWPP(I,J)=TWPP(I,J+1)=TWPP(I+1,J)=TWPP(I+1,J+1)=0.
      7     CONTINUE
            IF((TB(NPP)+T(NPP,1)).GE.TOP) PSI(NA,2)=TWPP(NA,2)=0.
            DO 8 J=2,MM
            IF((TB(NPP)+T(NPP,J)).GE.TOP) PSI(NA,J)=PSI(NA,J+1)
           + =TWPP(NA,J)=TWPP(NA,J+1)=0.
            WPPD(J)=TWPP(2,J)/(1.-PP*ABP(2))
      8     CONTINUE
      111   EPS=PSIMAX=0.
            IF(ITER.GE.ITMAX) GO TO 112
            ITER=ITER+1
            ITERS=ITERS+1
            GO TO (301,302,303,304),ITERS
      301   DO 305 J=2,MM
            OLDPSI=PSI(2,J)
            PSI(2,J)=WM*PSI(2,J)+WPPD(J)*(ABM(2)*PSI(3,J)+PSI(2,J+1)+PSI(2,
           + J-1)-ABT(2)*(T(2,J+1)-T(2,J-1)))
            CHANG=ABS(OLDPSI-PSI(2,J))
            IF(CHANG.GT.EPS) EPS=CHANG
            BOO=ABS(PSI(2,J))
            IF(BOO.GT.PSIMAX) PSIMAX=BOO
            DO 305 I=3,NA
            OLDPSI=PSI(I,J)
            PSI(I,J)=WM*PSI(I,J)+TWPP(I,J)*(ABM(I)*PSI(I+1,J)+ABP(I)*PSI(I-1,
           + J)+PSI(I,J+1)+PSI(I,J-1)-ABT(I)*(T(I,J+1)-T(I,J-1)))
            CHANG=ABS(OLDPSI-PSI(I,J))
            IF(CHANG.GT.EPS) EPS=CHANG
            BOO=ABS(PSI(I,J))
            IF(BOO.GT.PSIMAX) PSIMAX=BOO
      305   CONTINUE
            IF(EPS/PSIMAX-.0005) 112,111,111
      302   DO 306 JJ=2,MM $ J=M1-JJ
            DO 603 II=2,NZ $ I=NPPP-II
            OLDPSI=PSI(I,J)
            PSI(I,J)=WM*PSI(I,J)+TWPP(I,J)*(ABM(I)*PSI(I+1,J)+ABP(I)*PSI(I-1,
           + J)+PSI(I,J+1)+PSI(I,J-1)-ABT(I)*(T(I,J+1)-T(I,J-1)))
            CHANG=ABS(OLDPSI-PSI(I,J))
            IF(CHANG.GT.EPS) EPS=CHANG
            BOO=ABS(PSI(I,J))
            IF(BOO.GT.PSIMAX) PSIMAX=BOO
      603   CONTINUE
            OLDPSI=PSI(2,J)
            PSI(2,J)=WM*PSI(2,J)+WPPD(J)*(ABM(2)*PSI(3,J)+PSI(2,J+1)+PSI(2,
           + J-1)-ABT(2)*(T(2,J+1)-T(2,J-1)))
            CHANG=ABS(OLDPSI-PSI(2,J))
            IF(CHANG.GT.EPS) EPS=CHANG
            BOO=ABS(PSI(2,J))
            IF(BOO.GT.PSIMAX) PSIMAX=BOO
      306   CONTINUE
            IF(EPS/PSIMAX-.0005) 112,111,111
      303   DO 925 JJ=2,MM $ J=M1-JJ
            OLDPSI=PSI(2,J)
            PSI(2,J)=WM*PSI(2,J)+WPPD(J)*(ABM(2)*PSI(3,J)+PSI(2,J+1)+PSI(2,
           + J-1)-ABT(2)*(T(2,J+1)-T(2,J-1)))
            CHANG=ABS(OLDPSI-PSI(2,J))
            IF(CHANG.GT.EPS) EPS=CHANG
            BOO=ABS(PSI(2,J))
            IF(BOO.GT.PSIMAX) PSIMAX=BOO
      925   CONTINUE
            DO 307 I=3,NA
            DO 307 JJ=2,MM $ J=M1-JJ
```

Program listing (cont.)

```
150           OLDPSI=PSI(I,J)
              PSI(I,J)=WM*PSI(I,J)+TWPP(I,J)*(ABM(I)*PSI(I+1,J)+ABP(I)*PSI(I-1,
             + J)+PSI(I,J+1)+PSI(I,J-1)-APT(I)*(T(I,J+1)-T(I,J-1)))
              CHANG=ABS(OLDPSI-PSI(I,J))
              IF(CHANG.GT.EPS) EPS=CHANG
155           BOO=ABS(PSI(I,J))
              IF(BOO.GT.PSIMAX) PSIMAX=BOO
        307   CONTINUE
              IF(EPS/PSIMAX-.0005) 112,111,111
        304   DO 308 II=2,NZ
160           DO 308 J=2,MM
              I=NPP-II
              OLDPSI=PSI(I,J)
              PSI(I,J)=WM*PSI(I,J)+TWPP(I,J)*(ABM(I)*PSI(I+1,J)+ABP(I)*PSI(I-1,
             + J)+PSI(I,J+1)+PSI(I,J-1)-APT(I)*(T(I,J+1)-T(I,J-1)))
165           CHANG=ABS(OLDPSI-PSI(I,J))
              IF(CHANG.GT.EPS) EPS=CHANG
              BOO=ABS(PSI(I,J))
              IF(BOO.GT.PSIMAX) PSIMAX=BOO
        308   CONTINUE
170           DO 926 J=2,MM
              OLDPSI=PSI(2,J)
              PSI(2,J)=WM*PSI(2,J)+WPPD(J)*(ABM(2)*PSI(3,J)+PSI(2,J+1)+PSI(2,
             + J-1)-APT(2)*(T(2,J+1)-T(2,J-1)))
              CHANG=ABS(OLDPSI-PSI(2,J))
175           IF(CHANG.GT.EPS) EPS=CHANG
              BOO=ABS(PSI(2,J))
              IF(BOO.GT.PSIMAX) PSIMAX=BOO
        926   CONTINUE
              ITERS=0
180           IF(EPS/PSIMAX-.0005) 112,111,111
        112   DO 927 J=2,MM
        927   PSI(1,J)=PSI(2,J)
        C
        C VELOCITIES, TIME INTERVAL, AND PRINT-OUT CONTROL
185           DO 13 I=2,NA
              DO 113 J=1,MM
        113   U(I,J)=(PSI(I,J)-PSI(I,J+1))/DELY
              U(I,M)=U(I,MM)
        13    CONTINUE
190           DO 613 J=1,M
              U(1,J)=U(2,J)
        613   CONTINUE
              DO 713 I=2,NPP
              DO 713 J=2,MM
195     713   V(I,J)=(PSI(I,J)-PSI(I-1,J))/DELX
              VELMAX=0.
              DO 513 I=2,NPP
              DO 513 J=1,M
              A=ABS(U(I,J))+ABS(V(I,J))
200           IF(A.LE.VELMAX) GO TO 513
              VELMAX=A $ VM=V(I,J) $ UM=U(I,J)
        513   CONTINUE
              VD=SQRT(VM**2+UM**2)
              IF(VD.GT.D) D=VD
205           TDELT=SDELX/(DELX*VELMAX+4.)
              DELTAU=.9*TDELT
              TIME=TIME+DELTAU $ TIM=TIM+DELTAU
              IF(TIM.GT.TH63) GO TO 198
              IF(TIME.LT.TH1) GO TO 5000
210           XSES=TIME-TH1 $ DELTAU=DELTAU-XSES
              GO TO 4142
        198   IF(TIME.LT.TH3) GO TO 5000
              XSES=TIME-TH3 $ DELTAU=DELTAU-XSES
        4142  PRINT=1.
215           TIME=TIME-XSES $ TIM=TIM-XSES
        5000  CONTINUE
              NCNT=NCNT+1
        C
        C TEMPERATURES
220           C=DELTAU/DELX
              B=C/DELX
              TAP=DELTAU*ITT
              TNEW(N,1)=T(N,1)+B*(T(NL,1)+T(N,2)-2.*T(N,1))
              TNEW(N,M)=T(N,M)+B*(T(NL,M)+T(N,MM)-2.*T(N,M))
```

Program Listing (cont.)

```
225           DO 16 I=2,NL
              IF(U(I,1).GT.0.) UU=U(I,1)*(T(I-1,1)-T(I,1))
              IF(U(I,1).LE.0.) UU=U(I,1)*(T(I,1)-T(I+1,1))
              TNEW(I,1)=T(I,1)+B*(T(I+1,1)+T(I-1,1)+T(I,2)
             + -3.*T(I,1))+UU*C-TAP*U(I,1)
230           IF(U(I,M).GT.0.) UU=U(I,M)*(T(I-1,M)-T(I,M))
              IF(U(I,M).LE.0.) UU=U(I,M)*(T(I,M)-T(I+1,M))
              TNEW(I,M)=T(I,M)+B*(T(I,MM)+T(I-1,M)+T(I+1,M)
             + -3.*T(I,M))+UU*C-TAP*U(I,M)
              DO 16 J=2,MM
235           IF(U(I,J).LE.0.) UU=U(I,J)*(T(I,J)-T(I+1,J))
              IF(U(I,J).GT.0.) UU=U(I,J)*(T(I-1,J)-T(I,J))
              IF(V(I,J).LE.0.) VV=V(I,J)*(T(I,J)-T(I,J+1))
              IF(V(I,J).GT.0.) VV=V(I,J)*(T(I,J-1)-T(I,J))
        16    TNEW(I,J)=T(I,J)+B*(T(I+1,J)
240          + -4.*T(I,J)+T(I-1,J)+T(I,J+1)+T(I,J-1))+(UU+VV)*C-TAP*U(I,J)
              DO 15 J=2,MM
              IF(V(N,J).GT.0.) VV=V(N,J)*(T(N,J-1)-T(N,J))
              IF(V(N,J).LE.0.) VV=V(N,J)*(T(N,J)-T(N,J+1))
        15    TNEW(N,J)=T(N,J)+B*(T(NL,J)+T(N,J+1)+T(N,J-1)
245          + -3.*T(N,J))+VV*C
              QQQ=0.
              DO 222 J=1,M
        222   QQQ=QQQ+T(2,J)
              QQQQ=QQQ*DELTAU
250           QQT=QQT+QQQQ
              DO 17 I=2,N
              DO 17 J=1,M
        17    T(I,J)=TNEW(I,J)
        C
255     C AMOUNT OF CIRCULATION
              UP=DOWN=0. $ DO 3 J=1,M
              IF(U(1,J).GE.0.) GO TO 9
              UP=UP+U(1,J)
              GO TO 3
260     9     DOWN=DOWN+U(1,J)
        3     CONTINUE
              DOWN=(DOWN-UP)/2.
              DOWT=DOWT+(DOWN*DELTAU*500.)
              IF(PRINT.EQ.0.) GO TO 18
265           TDOWN=TDOWN+DOWT
              CDOWN=DOWN*5.E-4
        10    FORMAT (///* CIRCULATION = *F15.6* CM3/S/CM*////
             + * VOLUME OF CIRCULATION = *F15.6* CM3/CM*//)
              DOWT=0.
270     C
        C TOTAL HEAT
              SUMT=0.
              DO 777 J=1,M
              DO 777 I=2,N
275     777   SUMT=SUMT+T(I,J)
              SUMTT=SUMT*HOTT
        C
        C DIMENSIONS
              NTIM=TIM*3.8E5
280           DO 20 J=1,M
              DO 21 I=1,N
              NT(I,J)=TO*(T(I,J)+TB(I))
        21    CONTINUE
              DO 20 I=1,NPP
285           NU(I,J)=U(I,J)*2.5
              NV(I,J)=V(I,J)*2.5
        20    CONTINUE
              DD=D*2.5
        C
290           WRITE(6,23) NTIM,((NT(I,J),J=1,M),I=1,N)
        23    FORMAT (////*     AFTER*X,I5,X**YEARS:*////
             + * TEMPERATURE (DEG C)*///(1X,20(I4)//))
              WRITE(6,924) SUMTT
        924   FORMAT (/* TOTAL HEAT PERTURBATION = *F12.2* E+12 CAL/CM*/)
295     C
        C HEAT OUT
              OHEAT=QQT*HOT
              WRITE(6,889) OHEAT
        889   FORMAT (//* TOTAL HEAT OUT = *F10.6* E+12 CAL/CM*)
```

Program Listing (cont.)

```
300       C
          C CONDUCTIVE HEAT FLOW
                DO 41 J=1,M
          41    Q(J)=HT*T(2,J)
          C
305             WRITE(6,31) (Q(J),J=1,MM,2),(Q(J),J=2,M,2)
                + ,((PSI(I,J),J=1,M),I=1,NPP)
          31    FORMAT (////* SURFACE HEAT CONDUCTION (E-6 CAL/S CM2)*///
                + 1X,10(F5.1,3X)/4X,10(F5.1,3X)////* STREAM FUNCTION*
                + ///(1X,20(F4.2)//))
310             WRITE(6,4000) ITER
          4000  FORMAT (/* STREAM FUNCTION SCANS = *I2/)
                WRITE(6,32) DO,((NV(I,J),J=1,M),(NU(I,J),J=1,M),I=1,NPP)
          32    FORMAT (//* MAXIMUM VEL = *F8.2* E-8 CM/S*////
                + * HORIZONTAL AND VERTICAL VELOCITY FIELDS (E-8 CM/S) *//(/
315             + 1X,20(I4)/1X,20(I4)))
                WRITE(6,10) CDOWN,TDOWN
                WRITE(6,888) NCNT
          888   FORMAT (/* NUMBER OF COMPUTATION STEPS:   *I5)
          C
320       C TIMES
                D=TIME=PRINT=0
                NPRI=NPRI+1
                IF(NPRI.EQ.7) GO TO 444
                GO TO 18
325       444   STOP
                END
```

Sample Print-Out of Results

DYKE TEMP = 1200. DELX = .050 MAX PERM = .010
XPERM/YPERM = 1.0 DPERM/DX = -.01

AFTER 999 YEARS:

TEMPERATURE (DEG C) $(T_{i,j}^{\ell+1})$

0	0	0	0	0	0	0	0	0	0	0	0	0	0	0	0	0	0	0	0
326	217	106	44	23	19	19	19	19	19	19	19	19	19	19	19	19	19	19	19
505	348	176	78	46	39	39	39	39	39	39	39	39	39	39	39	39	39	39	39
590	407	213	102	66	59	59	59	59	59	59	59	59	59	59	59	59	59	59	59
623	426	232	122	86	79	79	79	79	79	79	79	79	79	79	79	79	79	79	79
639	456	252	141	106	99	99	99	99	99	99	99	99	99	99	99	99	99	99	99
649	470	270	160	126	119	119	119	119	119	119	119	119	119	119	119	119	119	119	119
659	483	287	180	146	139	139	139	139	139	139	139	139	139	139	139	139	139	139	139
669	493	304	199	166	160	159	159	159	159	159	159	159	159	159	159	159	159	157	159
679	512	322	218	186	180	179	179	179	179	179	179	179	179	179	179	179	179	179	179
690	525	339	238	205	200	199	199	199	199	199	199	199	199	199	199	199	199	199	199
700	538	357	257	225	220	219	219	219	219	219	219	219	219	219	219	219	219	219	219
710	552	374	276	245	240	239	239	239	239	239	239	239	239	239	239	239	239	239	239
720	565	391	295	265	260	259	259	259	259	259	259	259	259	259	259	259	259	259	259
730	578	408	315	285	280	279	279	279	279	279	279	279	279	279	279	279	279	279	279
740	592	425	334	305	300	299	299	299	299	299	299	299	299	299	299	299	299	299	299
751	605	442	353	325	320	319	319	319	319	319	319	319	319	319	319	319	319	319	319
761	619	460	372	345	340	339	339	339	339	339	339	339	339	339	339	339	339	339	339
773	633	477	392	365	360	359	359	359	359	359	359	359	359	359	359	359	359	359	359
789	650	496	412	385	380	380	379	379	379	379	379	379	379	379	379	379	379	379	379

TOTAL HEAT PERTURBATION = 5.42 E+12 CAL/CM $\{Q'(t^{\ell+1})$ [eq. (36)]}

TOTAL HEAT OUT = .266263 E+12 CAL/CM $\{Q'(t^{\ell+1})$ [eq. (35)]}

SURFACE HEAT CONDUCTION (E-6 CAL/S CM²) $[q_j'(t^{\ell+1})]$

153.0	43.4	1.9	-.4	-.3	-.2	-.2	-.2	-.1	-.1
98.5	12.5	-.2	-.3	-.3	-.2	-.2	-.1	-.1	-.1

Sample Print-Out of Results (cont.)

STREAM FUNCTION $(\psi^{\ell}_{i,j})$

0.00 .761.131.191.10 .97 .84 .72 .62 .53 .45 .38 .32 .26 .21 .16 .12 .08 .040.00

0.00 .761.131.191.10 .97 .84 .72 .62 .53 .45 .38 .32 .26 .21 .16 .12 .08 .040.00

0.00 .821.191.221.10 .96 .83 .72 .61 .52 .45 .38 .31 .26 .21 .16 .12 .08 .040.00

0.00 .841.201.211.08 .94 .81 .69 .60 .51 .43 .37 .31 .25 .20 .16 .12 .08 .040.00

0.00 .811.151.161.04 .89 .77 .66 .57 .49 .41 .35 .29 .24 .19 .15 .11 .07 .040.00

0.00 .741.071.08 .96 .83 .72 .62 .53 .45 .39 .33 .27 .23 .18 .14 .10 .07 .030.00

0.00 .63 .93 .96 .86 .75 .65 .56 .49 .42 .36 .30 .25 .21 .17 .13 .10 .06 .030.00

0.00 .44 .75 .81 .75 .66 .58 .50 .44 .38 .32 .27 .23 .19 .15 .12 .09 .06 .030.00

0.000.00 .52 .65 .63 .57 .50 .44 .39 .33 .29 .24 .21 .17 .14 .11 .08 .05 .030.00

0.000.00 .41 .53 .53 .48 .43 .38 .33 .29 .25 .21 .18 .15 .12 .09 .07 .05 .020.00

0.000.00 .34 .45 .44 .40 .36 .32 .28 .25 .21 .18 .15 .13 .10 .08 .06 .04 .020.00

0.000.00 .29 .37 .37 .34 .30 .27 .24 .21 .18 .15 .13 .11 .09 .07 .05 .03 .020.00

0.000.00 .24 .31 .30 .27 .25 .22 .19 .17 .15 .12 .11 .09 .07 .06 .04 .03 .010.00

0.000.00 .20 .25 .24 .22 .19 .17 .15 .13 .11 .10 .08 .07 .06 .04 .03 .02 .010.00

0.000.00 .16 .20 .19 .17 .15 .13 .11 .10 .09 .07 .06 .05 .04 .03 .02 .02 .010.00

0.000.00 .13 .15 .14 .12 .11 .09 .08 .07 .06 .05 .04 .04 .03 .02 .02 .01 .010.00

0.000.00 .09 .11 .10 .08 .07 .06 .05 .05 .04 .03 .03 .02 .02 .01 .01 .01 .000.00

0.000.00 .06 .07 .06 .05 .04 .03 .03 .02 .02 .02 .02 .01 .01 .01 .01 .00 .000.00

0.000.00 .03 .03 .02 .02 .02 .01 .01 .01 .01 .01 .01 .00 .00 .00 .00 .00 .000.00

0.000.000.000.000.000.000.000.000.000.000.000.000.000.000.000.000.000.000.00

STREAM FUNCTION SCANS = 25 (s)

MAXIMUM V+U = 41.74 E-8 CM/S $(|\overline{u}^{\ell}_{max}|)$

Sample Print-Out of Results (cont.)

HORIZONTAL AND VERTICAL VELOCITY FIELDS (E-8 CM/S) ($u^{\ell}_{y_{i,j}}$ and $u^{\ell}_{x_{i,j}}$)

```
  0   0   0   0   0   0   0   0   0   0   0   0   0   0   0   0   0   0   0   0
-38 -18  -2   4   6   6   5   5   4   4   3   3   2   2   2   2   2   2   1   1

  0   0   0   0   0   0   0   0   0   0   0   0   0   0   0   0   0   0   0   0
-38 -18  -2   4   6   6   5   5   4   4   3   3   2   2   2   2   2   2   1   1

  0   2   2   1   0   0   0   0   0   0   0   0   0   0   0   0   0   0   0   0
-40 -18  -1   5   7   6   5   5   4   3   3   3   2   2   2   2   2   1   1   1

  0   0   0   0   0  -1  -1  -1   0   0   0   0   0   0   0   0   0   0   0   0
-41 -18   0   6   7   6   5   4   4   3   3   3   2   2   2   2   1   1   1   1

  0  -1  -2  -2  -2  -2  -1  -1  -1  -1   0   0   0   0   0   0   0   0   0   0
-40 -17   0   6   7   6   5   4   4   3   3   2   2   2   2   1   1   1   1   1

  0  -3  -4  -4  -3  -3  -2  -2  -1  -1  -1  -1   0   0   0   0   0   0   0   0
-37 -16   0   5   6   5   4   4   3   3   2   2   2   2   2   1   1   1   1   1

  0  -5  -6  -6  -4  -3  -3  -2  -2  -1  -1  -1  -1   0   0   0   0   0   0   0
-31 -15  -1   4   5   4   4   3   3   3   2   2   2   2   1   1   1   1   1   1

  0  -9  -9  -7  -5  -4  -3  -2  -2  -2  -1  -1  -1   0   0   0   0   0   0   0
-21 -15  -2   3   4   4   3   3   2   2   2   2   1   1   1   1   1   1   1   1

  0 -21 -11  -7  -5  -4  -3  -3  -2  -2  -1  -1  -1  -1   0   0   0   0   0   0
  0 -25  -6   1   3   3   3   2   2   2   2   1   1   1   1   1   1   1   1   1

  0   0  -5  -5  -5  -4  -3  -3  -2  -2  -1  -1  -1  -1   0   0   0   0   0   0
  0 -20  -6   0   2   2   2   2   2   1   1   1   1   1   1   1   1   1   1   1

  0   0  -3  -4  -4  -3  -3  -2  -2  -2  -1  -1  -1  -1   0   0   0   0   0   0
  0 -17  -5   0   1   2   2   1   1   1   1   1   1   1   1   1   1   0   1   1

  0   0  -2  -3  -3  -3  -3  -2  -2  -2  -1  -1  -1  -1   0   0   0   0   0   0
  0 -14  -4   0   1   1   1   1   1   1   1   1   1   1   0   0   0   0   0   0

  0   0  -2  -3  -3  -3  -2  -2  -2  -1  -1  -1  -1  -1   0   0   0   0   0   0
  0 -12  -3   0   1   1   1   1   1   1   1   0   0   0   0   0   0   0   0   0

  0   0  -2  -2  -2  -2  -2  -2  -2  -1  -1  -1  -1   0   0   0   0   0   0   0
  0  -9  -2   0   1   1   1   1   0   0   0   0   0   0   0   0   0   0   0   0

  0   0  -1  -2  -2  -2  -2  -2  -1  -1  -1  -1  -1   0   0   0   0   0   0   0
  0  -8  -2   0   1   1   0   0   0   0   0   0   0   0   0   0   0   0   0   0

  0   0  -1  -2  -2  -2  -2  -1  -1  -1  -1  -1   0   0   0   0   0   0   0   0
  0  -6  -1   0   0   0   0   0   0   0   0   0   0   0   0   0   0   0   0   0

  0   0  -1  -2  -2  -2  -1  -1  -1  -1  -1   0   0   0   0   0   0   0   0   0
  0  -4   0   0   0   0   0   0   0   0   0   0   0   0   0   0   0   0   0   0

  0   0  -1  -2  -1  -1  -1  -1  -1  -1   0   0   0   0   0   0   0   0   0   0
  0  -2   0   0   0   0   0   0   0   0   0   0   0   0   0   0   0   0   0   0

  0   0  -1  -1  -1  -1  -1  -1   0   0   0   0   0   0   0   0   0   0   0   0
  0  -1   0   0   0   0   0   0   0   0   0   0   0   0   0   0   0   0   0   0

  0   0  -1  -1  -1   0   0   0   0   0   0   0   0   0   0   0   0   0   0   0
  0   0   0   0   0   0   0   0   0   0   0   0   0   0   0   0   0   0   0   0
```

CIRCULATION = .012076 CM3/S/CM {$C(t^{\ell})$ [eq. (37)]}

VOLUME OF CIRCULATION = 15.661772 CM3/CM {$V(t^{\ell})$ [eq. (38)]}

NUMBER OF COMPUTATION STEPS: 5 (ℓ-1)

BIBLIOGRAPHY

Ballard, R. D. (1975). Project FAMOUS II: Dive into the great rift, Nat. Geogr. 147, 604-615.

Bellaiche, G., J. L. Cheminee, J. Francheteau, R. Hekinian, X. Le Pichon, N. D. Needham, and R. D. Ballard (1974). Rift valley's inner floor: First submersible study, Nature 250, 558-560.

Bodvarsson, G., and R. P. Lowell (1972). Ocean-floor heat flow and circulation of interstitial waters, J. Geophys. Res. 77, 4472-4475.

Carnahan, B., H. A. Luther, and J. O. Wilkes (1969). Applied Numerical Methods, John Wiley and Sons, New York.

Dietz, R. S. (1961). Continent and ocean basin evolution by spreading of the sea floor, Nature 190, 854-857.

Donaldson, I. G. (1962). Temperature gradients in the upper layers of the earth's crust due to convective water flows, J. Geophys. Res. 67, 3449-3459.

Dusinberre, G. M. (1961). Heat Transfer Calculations by Finite Differences, International Textbooks, Scranton.

Elder, J. W. (1966). Numerical experiments with free convection in a vertical slot, J. Fluid Mech. 24, 823-843.

Elder, J. W. (1966). Transient convection in a porous medium, J. Fluid Mech. 27, 609-623.

Hess, H. H. (1962). History of ocean basins, Petrologic Studies: A Volume to Honor A. F. Buddington, Geological Society of America, pp. 599-620.

Holst, P. H., and K. Aziz (1972a). A Theoretical and experimental study of natural convection in a confined porous medium, Can. J. Chem. Eng. 50, 232-241.

Holst, P. H., and K. Aziz (1972b). Transient three-dimensional natural convection in confined porour media, Int. J. Heat Mass Transfer 15, 73-90.

Horne, R. N., and M. J. O'Sullivan (1974). Oscillatory convection in a porous medium heated from below, J. Fluid Mech. 66, 339-352.

Irving, E. (1970). The Mid-Atlantic Ridge at 45°N: XIV. Oxidation and magnetic properties of basalt (review and discussion), Can. J. Earth Sci. 7, 1528-1538.

Irving, E., J. K. Park, S. E. Haggerty, F. Aumento, and B. Loncarevic (1970). Magnetism and opaque mineralogy of basalts from the Mid-Atlantic Ridge at 45°N., Nature 228, 974-976.

Langseth, M. G., X. Le Pichon, and M. Ewing (1966). Crustal structure of the mid-ocean ridges: 5. Heat flow through the Atlantic Ocean floor and convection currents, J. Geophys. Res. 71, 5321-5355.

Lapwood, E. R. (1948). Convection of a fluid in a porous medium, Proc. Cambridge Phil. Soc. 44, 508-521.

Lee, W. H. K., and S. Uyeda (1965). Review of heat flow data, Terrestrial Heat Flow: Geophysical Monograph 8, American Geophysical Union, Washington, pp. 87-190.

Lister, C. R. B. (1972). On the thermal balance of a mid-ocean ridge, Geophys. J. Roy. Astron. Soc. 26, 515-535.

Lister, C. R. B. (1974). On the penetration of water into hot rock, Geophys. J. Roy. Astron. Soc. 39, 465-509.

Lowell, R. P. (1975). Circulation in fractures, hot springs, and convective heat transport on mid-ocean ridge crests, Geophys. J. Roy. Astron. Soc. 40, 351-365.

McKenzie, D. P. (1967). Some remarks on heat flow and gravity anomalies, J. Geophys. Res. 72, 6261-6273.

Moore, J. G., H. S. Fleming, and J. D. Phillips (1974). Preliminary model for extrusion and rifting at the axis of the Mid-Atlantic Ridge, 36°48' North, Geology 2, 437-440.

Muskat, M. (1937). The Flow of Homogeneous Fluids through Porous Media, McGraw Hill, New York.

Neumann, G., and W. J. Pierson, Jr. (1966). Principles of Physical Oceanography, Prentice-Hall, Englewood Cliffs.

Nield, D. A. (1968). Onset of thermohaline convection in a porous medium, Water Resour. Res. 4, 553-560.

Oldenburger, R. (1940). Infinite powers of matrices and characteristic roots, Duke Math. J. 6, 357-361.

Pálmason, G. (1967). On the heat flow in Iceland in relation to the Mid-Atlantic Ridge, Iceland and Mid-Ocean Ridges, "RIT" 38, Societas Scientiarum Islandica, Reykjavik, pp. 111-127.

Parker, R. L., and D. W. Oldenburg (1973). Thermal models of ocean ridges, Nature 242, 137-139.

Revelle, R., and A. E. Maxwell (1952). Heat flow through the floor of the eastern north Pacific Ocean, Nature 170, 199-200.

Ribando, R. J., K. E. Torrance, and D. L. Turcotte (1976). Numerical models for hydrothermal circulation in the oceanic crust, J. Geophys. Res. 81, 3007-3012.

Richter, F. M. (1973). Dynamic models for sea-floor spreading, Rev. Geophys. Space Phys. 11, 223-287.

Rona, P. A., B. A. McGregor, P. R. Betzer, G. W. Bolger, and D. C. Krause (1975). Anomalous water temperatures over the Mid-Atlantic Ridge crest at 26°N latitude, Deep-Sea Res. 22, 611-618.

Sclater, J. G., and J. Francheteau (1970). The implications of terrestrial heat flow observations on current tectonic and geochemical models of the crust and upper mantle of the earth, Geophys. J. Roy. Astron. Soc. 20, 509-542.

Sleep, N. H. (1969). Sensitivity of heat flow and gravity to the mechanisms of sea-floor spreading, J. Geophys. Res. 74, 542-549.

Spooner, E. T. C., and W. S. Fyfe (1973). Sub-sea-floor metamorphism heat and mass transfer, Contr. Mineral Petrol. 42, 287-304.

Straus, J. M. (1974). Large amplitude convection in porous media, J. Fluid Mech. 64, 51-63.

Sykes, L. R. (1971). Earthquake swarms and sea-floor spreading, J. Geophys. Res. 75, 6598-6611.

Talwani, M., C. C. Windisch, and M. G. Langseth, Jr. (1971). Reykjanes ridge crest: A detailed geophysical study, J. Geophys. Res. 76. 473-517.

Torrance, K. E. (1968). Comparison of finite-difference computations of natural convection, J. Res. Nat. Bur. Stand. 72B, 281-301.

Von Herzen, R. P. (1959). Heat flow values from the south-eastern Pacific, Nature 183, 882-883.

Von Herzen, R. P., and M. G. Langseth (1966). Present status of oceanic heat-flow measurements, Phys. Chem. Earth 6, 365-407.

Williams, D. L., R. P. Von Herzen, J. G. Sclater, and R. N. Anderson (1974). Galapagos Spreading Center: Lithospheric cooling and hydrothermal circulation, Geophys. J. Roy. Astron. Soc. 38, 587-608.

Wolery, T. J., and N. H. Sleep (1975). Hydrothermal circulation and geochemical flux at mid-ocean ridges (submitted to) J. Geol.

Young, D. (1954). Iterative methods for solving partial difference equations of elliptic type, Trans. Am. Math. Soc. 76, 92-111.